AD-A249 868

ITATION PAGE

ᵖᵈ to average 1 hour per response, including the time for reviewing instructions, searching existing data sources,
viewing the collection of information. Send comments regarding this burden estimate or any other aspect of this
rden to Washington Headquarters Services, Directorate for Information Operations and Reports, 1215 Jefferson
ᵗʰⁱᶜ of Management and Budget, Paperwork Reduction Project (0704-0188), Washington, DC 20503

1. AGENCY USE ONLY (Leave blank)	2. REPORT DATE 1991	3. REPORT TYPE AND DATES COVERED THESIS/~~DISSERTATION~~

4. TITLE AND SUBTITLE	5. FUNDING NUMBERS
High-Latitude Spacecraft Charging In Low-Earth Polar Orbit	

6. AUTHOR(S)

Thomas B. Frooninckx, Capt

7. PERFORMING ORGANIZATION NAME(S) AND ADDRESS(ES)	8. PERFORMING ORGANIZATION REPORT NUMBER
AFIT Student Attending: Utah State University	AFIT/CI/CIA-91-119

9. SPONSORING/MONITORING AGENCY NAME(S) AND ADDRESS(ES)	10. SPONSORING/MONITORING AGENCY REPORT NUMBER
AFIT/CI Wright-Patterson AFB OH 45433-6583	

11. SUPPLEMENTARY NOTES

12a. DISTRIBUTION/AVAILABILITY STATEMENT	12b. DISTRIBUTION CODE
Approved for Public Release IAW 190-1 Distributed Unlimited ERNEST A. HAYGOOD, Captain, USAF Executive Officer	

13. ABSTRACT (Maximum 200 words)

DISTRIBUTION STATEMENT A
Approved for public release
Distribution Unlimited

DTIC
ELECTE
MAY 11 1992
S B D

14. SUBJECT TERMS			15. NUMBER OF PAGES 100
			16. PRICE CODE

17. SECURITY CLASSIFICATION OF REPORT	18. SECURITY CLASSIFICATION OF THIS PAGE	19. SECURITY CLASSIFICATION OF ABSTRACT	20. LIMITATION OF ABSTRACT

HIGH-LATITUDE SPACECRAFT CHARGING

IN LOW-EARTH POLAR ORBIT

by

Thomas B. Frooninckx

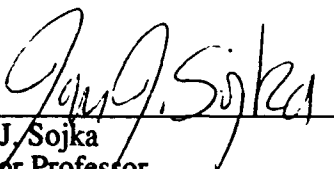A thesis submitted in partial fulfillment
of the requirements for the degree

of

MASTER OF SCIENCE
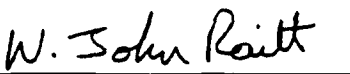
in
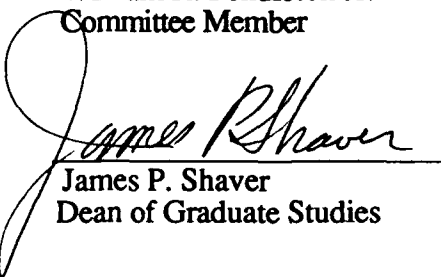
Physics
(Upper Atmospheric Option)

Approved:

Jan J. Sojka
Major Professor

William R. Pendleton Jr.
Committee Member

W. John Raitt
Committee Member

James P. Shaver
Dean of Graduate Studies

UTAH STATE UNIVERSITY
Logan, Utah

1991

ACKNOWLEDGEMENTS

<div align="right">T. Frooninckx</div>

TABLE OF CONTENTS

LIST OF TABLES

LIST OF FIGURES

ABSTRACT

High-Latitude Spacecraft Charging

In Low-Earth Polar Orbit

by

Thomas B. Frooninckx, Master of Science

Utah State University, 1991

Major Professor: Dr. Jan J. Sojka
Department: Physics

Spacecraft charging within the upper ionosphere is commonly thought to be insignificant and thus has received little attention. Recent experimental evidence has shown that electric potential differences as severe as -680 volts can develop between Defense Meteorological Satellite Program (DMSP) polar-orbiting (840 kilometers) spacecraft and their high-latitude environment. To explore space vehicle charging in this region more fully, an analysis was performed using DMSP F6, F7, F8, and F9 satellite precipitating particle and ambient plasma measurements taken during the winters of 1986-87 (solar minimum) and 1989-90 (solar maximum).

An extreme solar cycle dependence was discovered as charging occurred more frequently and with greater severity during the period of solar minimum. One hundred seventy charging events ranging from -46 to -1,430 volts were identified, and satellite measurements and Time Dependent Ionospheric Model (TDIM) output were used to characterize the environments which generated and inhibited these potentials. All current sources were considered to determine the cause of the solar cycle dependence.

The examination of precipitating electron populations associated with various DMSP charging levels suggested that electrons greater than 2 keV can contribute to a

92-11942

02 5 01 032

negative charge imbalance, but the greatest contributions were frequently made by the more energetic ($\geq$9.6 keV) electrons. Secondary electron production due to incident electrons below 1 keV inhibited negative charging. The energetic electron fluxes shown to generate charging did not vary significantly between solar maximum and minimum. Instead, DMSP and TDIM ambient plasma data indicated that a variation in plasma density over one or more orders of magnitude caused the solar cycle dependence, and a plasma density of less than 10^4 cm^{-3} was found necessary for significant negative charging ($\geq$100 volts) to occur. (110 pages)

CHAPTER I

INTRODUCTION

The growing utilization of space for communicative, experimental, and other military and commercial purposes demands an understanding of the environments which limit system performance. Complex interactions between the sun, interplanetary space, and the earth's magnetic field and atmosphere generate physical, chemical, and electrodynamic processes which can adversely affect an orbiting vehicle. One electrodynamic process which requires attention is the accumulation of electrical charge on a satellite's surface.

Spacecraft charging studies during the past twenty years have primarily focused on the most severe charging environments. The space physics community has aggressively documented the causes and effects of spacecraft charging at geosynchronous orbit altitudes ($\approx$36,000 kilometers), where negative charging levels can reach multi-kilovolts and cause significant operational anomalies. Less attention has been given to spacecraft charging at low-earth orbit altitudes (<1000 kilometers), where electric potential differences between satellites and their environments are thought to be insignificant. This investigation aims to enhance the understanding of spacecraft charging at these lower altitudes.

The primary causes, frequency, severity, and solar cycle dependence of spacecraft charging within the high-latitude upper ionosphere are identified using satellite measurements taken in 840-kilometer circular polar orbit. The study's data base consists of two sets of northern hemispheric measurements, one from the winter of 1986-1987 and the other from the winter of 1989-1990, which represent solar minimum and maximum conditions, respectively. The data sets are examined in detail to identify all negative charging events more severe than -45 volts, and an analysis of

the environments which generate and inhibit charging is perform ...

The presentation of this study begins in Chapter II with a definition, historical review, and theoretical analysis of spacecraft charging and includes a brief discussion of charging effects and computer modeling efforts. Chapter III identifies the Defense Meteorological Satellite Program spacecraft which provide data for this study, and a detailed description of the satellites' instrumentation is given. Chapter IV presents the results of a previous survey of high-latitude spacecraft charging and serves as a quantitative foundation for Chapters V (solar maximum) and VI (solar minimum) which describe the data bases, analytical methods, and results of this investigation. A discussion of the results is given in Chapter VII, and finally, conclusions and recommendations for further study are listed in Chapter VIII.

CHAPTER II

HISTORICAL AND THEORETICAL PERSPECTIVE

2.1 Definition

Spacecraft charging occurs when positive or negative particles accumulate on or are removed from a space vehicle's surface such that a net charge imbalance induces an electric potential difference between the spacecraft and surrounding neutral plasma. The differential form of Gauss's law describes the electric field $(\vec{E})$ due to a charged object,

$$\vec{\nabla} \cdot \vec{E} = \frac{\rho}{\varepsilon_0} \ , \tag{1}$$

where ρ is the net charge density, and ε_0 is the permittivity of free space. Since the negative gradient of the electric potential (ϕ) also describes an electric field,

$$\vec{E} = -\vec{\nabla}\phi \ , \tag{2}$$

then a substitution for $\vec{E}$ into Equation (1) provides a description of the electric potential distribution in the form of Poisson's equation,

$$\nabla^2 \phi = -\frac{\rho}{\varepsilon_0} \ . \tag{3}$$

The use of equation (3) to describe the potential distribution of a charged spacecraft is made difficult if a plasma surrounds the spacecraft.

The potential distribution due to a charged spacecraft does not extend indefinitely into space. Instead, the potential is confined to a region of charged particles opposite in

polarity to the charged spacecraft which effectively cancels the distant electrostatic effects of the vehicle's charge imbalance. This region is known as a charge sheath, and its size is largely a function of ambient plasma density and satellite potential. For a sphere with a radius of three meters and charged to one kilovolt in low-earth orbit, sheath thickness estimates range from 2.5 to 5.0 meters [*Laframboise*, 1983]. An ideal charge sheath for a negatively charged, spherically symmetric conductor is depicted in Figure 1. Realistically, such a simplistic characterization is valid only at a constant charging level, when the surrounding plasma has had time to rearrange in response to the charged object. The sheath is not easily described when spacecraft charging levels change rapidly, and few experimental studies have attempted to quantitatively describe this feature. In the high-latitude upper ionosphere, measured potential levels typically change over hundreds of volts in one second [*Gussenhoven et al.*, 1985], and theoretical time constants for a 1-kilovolt potential to form on a sphere of 1-meter radius range from 0.002 seconds (conductor) to 1.6 seconds (dielectric) [*Katz et al.*, 1977b]. Most often, spacecraft-charging studies have focused on the processes which cause significant surface charge imbalances.

A spacecraft-to-plasma potential difference generated by natural sources within the space environment is defined as passive spacecraft charging, while a charge imbalance achieved by artificial means is classified as active charging. To begin this study of passive spacecraft charging within the low-earth orbit (LEO) polar environment, a brief review of the more significant charging studies is presented. The natural charging sources are then introduced as part of a current balance equation, and each term is described relative to the LEO polar environment. Finally, after the major effects of spacecraft charging are identified, model predictions of auroral-caused Space Shuttle charging are presented.
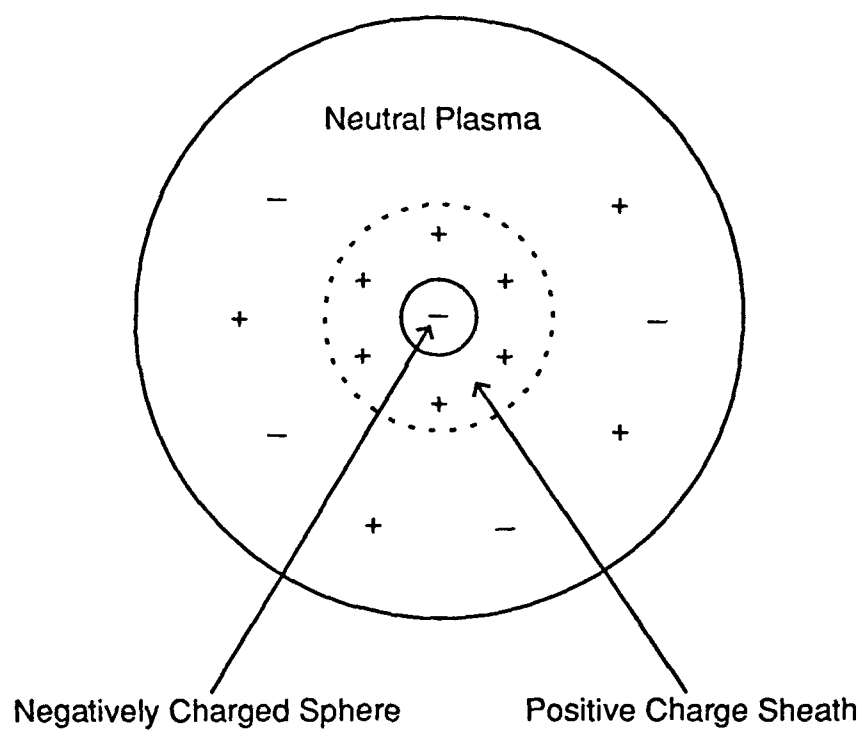
Fig. 1. Charge sheath for symmetrically charged sphere in the presence of a plasma.

2.2 Previous Charging Studies

The theoretical foundation of spacecraft charging analysis is most often attributed to Langmuir's electrostatic probe work during the early twentieth century [*Langmuir and Blodgett*, 1924]. The theoretical studies which soon followed considered the charging of interstellar dust grains, but the focus of study changed to spacecraft charging during the 1950's and 1960's with the development of rockets and satellites. Interest became widespread, and numerous predictions and measurements of spacecraft potentials soon followed. A detailed review of the spacecraft charging studies of this earlier period is given by *Garrett* [1981]. By 1965, many of the sources of spacecraft charging had been identified, and several rockets and satellites had measured charging levels ranging from +10 volts to -20 volts within the earth's ionosphere. These electric potentials were incomparable to those experienced by the geosynchronous Applied Technology Satellite 5 (ATS-5) in 1969.

2.2.1 Geosynchronous Orbit Charging

The identification of negative potentials as severe as -10 kilovolts on the ATS-5 [*DeForest*, 1972] was a major discovery in the study of spacecraft charging. After a launch into a 2.3 degree inclination geosynchronous orbit in August 1969, the ATS-5 plasma detector recorded sudden changes in the proton spectral shape when the satellite entered the earth's shadow while moving through the plasma sheet. DeForest concluded from the electron and ion spectra that the satellite was charging negatively (typically -3000 volts to -4000 volts), primarily due to the bombardment of energetic electrons during a magnetic substorm. (DeForest's method of identifying charging is used in this study and is described in section 5.2). The launch of a second geosynchronous satellite (ATS-6) in 1974 provided another vehicle to study spacecraft charging, and the ATS-6 subsequently developed the most severe potential (-19,000

volts) ever reported on a satellite [*Olsen*, 1987]. The discovery of large negative electric potentials in the low density plasma sheet mobilized the space physics and engineering communities to investigate further the spacecraft charging phenomenon. The United States Air Force and the National Aeronautics and Space Administration (NASA) launched the Spacecraft Charging at High Altitudes (SCATHA) P78-2 satellite in 1979 to specifically study charging at near-geosynchronous altitudes.

Like the ATS-5, the P78-2 experienced significant negative potentials while in eclipse within the plasma sheet during an injection of high energy electrons. *Gussenhoven and Mullen* [1983] reported P78-2 charging levels as severe as -8000 volts in eclipse and -340 volts in sunlight and determined that the satellite would have charged to more than -15 kilovolts had the sunlight charging environment been present during eclipse. *Olsen* [1983] found that the ATS and SCATHA satellites charged in eclipse only if plasma sheet electron fluxes extended above 10 keV, and *Mullen et al.* [1986] labeled 30 keV as a key electron energy necessary to produce significant negative charging in sunlight. While the ATS and SCATHA experiments demonstrated that the near-geostationary environment was clearly conducive to charging, studies of the ionospheric/LEO environment have reported less severe charging levels.

2.2.2 Low-Earth Orbit Charging

The most recent studies of spacecraft charging in low-earth orbit include that of high-latitude Defense Meteorological Satellite Program F6 and F7 satellite charging [*Gussenhoven et al.*, 1985] and low- to mid-latitude Space Shuttle charging [*Raitt et al.*, 1987]. Since the low- to mid-latitude environment at shuttle orbiting altitudes (225 -350 kilometers) is normally conducive only to insignificant passive charging (less than -10 volts), the Space Shuttle Vehicle Charging and Potential experiments actively charged the shuttle to positive potentials using an electron gun. The experiments were chiefly designed to evaluate the induced positive potential and monitor any

perturbations to the potential distribution around the shuttle. In contrast, *Gussenhoven et al.* [1985] found the polar regions near 800 kilometers to be more conducive to passive negative charging where electric potentials on the Defense Meteorological Satellite Program spacecraft reached -680 volts, and as found in the geosynchronous studies, the significant charging occurred in darkness during energetic electron precipitation. (The study by *Gussenhoven et al.* [1985] is described further in Chapter IV). To understand why charging levels vary depending on environment, an examination of the current to and from a spacecraft is necessary.

2.3 Sources of Charging

A charge imbalance on a spacecraft's surface is the result of anisotropic currents (J) to and from the vehicle. The sources of these currents may include:

ambient electrons (J_e)

ambient ions (J_i)

energetic electrons of magnetospheric origin (J_{em})

energetic ions of magnetospheric origin (J_{im})

secondary electrons from energetic electrons (J_{2ee})

secondary electrons from energetic ions (J_{2ei})

backscattered electrons (J_{be})

secondary ions from energetic electrons (J_{2ie})

secondary ions from energetic ions (J_{2ii})

backscattered ions (J_{bi})

photoemission (J_{ph})

A spacecraft's potential varies until current balance to and from the vehicle is attained such that:

$$J_i + J_{im} + J_{ph} + J_{2ee} + J_{2ei} + J_{be} = J_e + J_{em} + J_{2ie} + J_{2ii} + J_{bi} \quad . \qquad (4)$$

The nature of these terms within the LEO polar environment suggests which current sources are dominant.

2.3.1 Ambient Plasma

In the absence of a spacecraft-to-plasma potential difference, the currents due to ambient electrons and ions impacting a spacecraft's surface are nearly self balancing; that is, $J_i \approx J_e$. The slight inequality is due to the different thermal speeds of the electrons and ions. Greater ambient electron thermal speeds result in a greater electron current to the spacecraft and a negative surface charge imbalance. However, once a negative charge imbalance forms, the resulting electric field repels electrons and attracts ions such that the ambient ion and electron currents become equal. This process is magnified within the plasma wake on the trailing edge of an orbiting spacecraft. Ambient electrons have access to a satellite through the wake region since their velocities are greater than typical orbital velocities in LEO (~8 kilometers/second), but the ambient ions' velocities are normally slower than the orbital velocity, so their curres t is primarily confined to the ram side of the spacecraft. As already noted, an accumulation of electrons in this manner is self-limiting; once electrons begin to collect within the wake region, a negative potential develops and repels additional electrons from entering. The overall charge imbalance created by these processes produces an insignificant negative potential. In the presence of a significant current from another source, the ambient electrons or ions can play a key role in maintaining current balance.

If other currents generate a negative spacecraft potential, the resulting electric field will accelerate ambient ions toward the vehicle until a charge balance results. At upper ionospheric altitudes and high latitudes, plasma densities normally range from 10^2-10^5 cm^{-3}, so this balancing resource is relatively plentiful. At geosynchronous altitudes within the plasma sheet where charging is often severe, the plasma density is ≤ 1 cm^{-3}, so fewer particles exist which can neutralize a charged spacecraft. While ambient ion

and electron currents in LEO are virtually equal and opposite in the absence of other currents, precipitating energetic electron and ion currents are not.

2.3.2 Precipitating Particles

Energetic electrons and ions of magnetospheric origin have access to spacecraft in the LEO polar environment through magnetic field-aligned precipitation. Since electron and ion precipitation are not necessarily simultaneous, the terms J_{em} and J_{im} are non-balancing and may cause a spacecraft's potential to vary significantly. Extensive statistical studies of high-latitude electron and ion precipitation at 840 kilometers [*Hardy et al.*, 1985; *Hardy et al.*, 1989] show the average number flux of precipitating electrons with energies between 30 eV-30 keV to be 10 to 100 times greater than precipitating ion fluxes at similar energies for all latitudes, magnetic local times, and magnetic activities. Hence, electron precipitation is most often a more dominant current source though ion precipitation cannot be totally discounted. Both precipitating electrons and ions create additional terms in the current balance equation.

2.3.3 Backscattered and Secondary Particles

Precipitating electrons and ions impacting a spacecraft's surface may backscatter or create secondary electrons or ions which leave the spacecraft's surface. Because precipitating electron number fluxes are greater, backscattered electrons and electron created secondaries are particularly pertinent to current balance. The number of backscattered electrons is only a fraction of the total number of incident primaries normal to the surface, equaling less than one tenth at most energies for a spacecraft material like kapton [*Katz et al.*, 1977a; *Prokopenko and Laframboise*, 1980]. In contrast, the number of secondary electrons created by a precipitating electron is a function of the precipitating electron's energy [*Katz et al.*, 1977a; *Leung et al.*, 1981], so the secondary electron current is not necessarily determined by the number of precipitating electrons. Figure 2 depicts the ratio of secondary electrons to primary
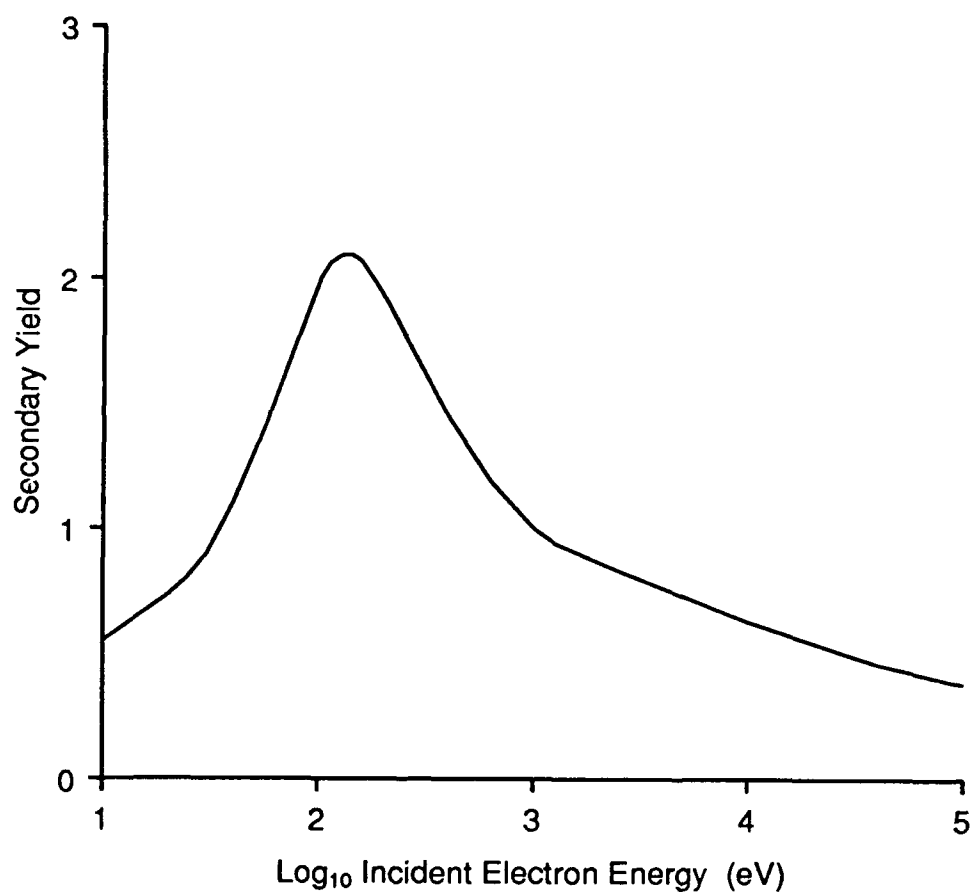
Fig. 2. Secondary electron yield coefficients for kapton due to incident electrons normal to surface (after *Katz et al.*, 1977a).

electrons for kapton (the primary material of the Defense Meteorological Satellite Program spacecraft) as a function of the primary's energy. This function identifies lower energy precipitating electrons as being self-balancing and is consistent with the experimental result that higher energy electrons rather than all electrons are the primary cause of significant negative potentials [*DeForest*, 1972; *Gussenhoven et al.*, 1985; *Mullen et al.*, 1986]. While backscattered precipitating ions, ion generated secondaries, and electron generated secondary ions are not important to current balance in the upper ionosphere [*Garrett*, 1981; *Yeh and Gussenhoven*, 1987], the remaining term in the current balance equation is quite significant.

2.3.4 Photoemission

Photoemission is the removal of electrons from a spacecraft's surface due to photon impact and, therefore, inhibits negative potentials from occurring in sunlight. While varying with surface orientation, material, and solar intensity, the photoemission current is approximately 100 times greater than auroral electron created secondary electron currents [*Raitt et al.*, 1987]. Quantifying photoemission is difficult since it only occurs on the sunlit side of a spacecraft and can be suppressed by an asymmetrical electric potential distribution around a charged body [*Whipple*, 1976; *Besse and Rubin*, 1980; *Whipple and Olsen*, 1987]. Other effects exist which modify all of the currents to and from a spacecraft.

2.3.5 Magnetic and Electric Field Effects

The geomagnetic field within the LEO environment can alter the natural source currents. The direction of the magnetic field relative to a spacecraft's surface determines the ease with which charged particles move to and from the spacecraft. The escape of backscattered and secondary electrons and photoelectrons is inhibited if the magnetic field is parallel to the surface. Thorough descriptions of this effect are given

by *Laframboise* [1983] and *Laframboise and Parker* [1987].

An electric field may be generated on a satellite's surface as a result of the satellite with velocity ($\vec{V}$) moving through a magnetic field ($\vec{B}$) [*Whipple*, 1983]. The electric field is generated from $\vec{V} \times \vec{B}$ and is relatively insignificant on normal size satellites, but the effect has been observed on the Space Shuttle [*Raitt*, 1983], and the maximum $\vec{V} \times \vec{B}$ electric field for a spacecraft in LEO is approximately 0.25-0.50 volts/meter [*Grard et al.*, 1983a; *Raitt et al.*, 1987] depending on the type of orbit; the $\vec{V} \times \vec{B}$ effect is increased for larger vehicles. Of course, the magnetic and electric field effects and all of the current balance terms may be working simultaneously, and the net result determines whether a potential is created, and once created, whether it varies. If a significant potential forms, the effects on the satellite become of concern.

2.4 Spacecraft Charging Effects

Generally, an electric potential difference between a spacecraft and its plasma environment is not by itself damaging to space systems, but since space vehicles often consist of materials which are poor conductors, and the source currents are anisotropic, differential surface charging can cause serious anomalies. Differential charging is the unequal charge distribution throughout a spacecraft's surface, and this phenomenon is believed to be responsible for the complete failure of a spacecraft [*Shaw et al.*, 1976]. Dielectric surface charging contributes to arc discharges and electromagnetic interference which can result in component failure [*Rosen*, 1976; *Balmain*, 1987], and differential charging between shadowed and sunlit nonconducting surfaces can be particularly severe. The development of electrostatically clean satellites has met with some success in inhibiting spacecraft-to-plasma and differential potentials from forming [*Whipple and Olsen*, 1987; *Broihanne*, 1987]. A review of spacecraft charging effects is presented by *Grard et al.* [1983b], and over 80 references concerning charging effects are cited by *Balmain* [1987]. Efforts to model differential charging are given by

Parker [1978], *Prokopenko and Laframboise* [1980], and *Katz and Mandell* [1982]. Measurements which demonstrate the ability of differential charging to generate a potential barrier which can trap particles emitted from a spacecraft's surface are presented in *Garrett and DeForest* [1979], *Olsen et al.* [1981], and *Whipple and Olsen* [1987]. While these effects occurred at geosynchronous altitudes where charging is more severe, concern exists that differential charging would likewise be damaging to large space systems in polar LEO, and present day modeling efforts support this concern.

2.5 Charging Models and Predictions

The possibility of a Space Shuttle mission in polar orbit brought an urgency in predicting what potential levels the orbiter would develop at high latitudes. Though a Space Shuttle orbit over the poles now appears to be several years away, the modeling efforts are not wasted as additional systems continue to launch into polar LEO. Since spacecraft in the same environment may charge to different levels depending on their size, shape, and material, an assumption that a large body in polar orbit would achieve potentials similar to that of smaller satellites is not valid. The NASA Charging Analyzer Program was developed to simulate charging of a spacecraft in geosynchronous orbit and has since led to codes that predict spacecraft charging within the upper ionosphere.

Parks and Katz [1981] used a simplified spherical model of the Space Shuttle and calculated that the orbiter would charge to -1000 volts relative to its 200-400 kilometer polar environment during auroral conditions and could also charge differentially up to -1000 volts. Most recently, *Hall et al.* [1987] reported that the POLAR charging code, which considers various geometrical shapes, surfaces, photoemission, and secondary behavior, calculates that the shuttle would charge to thousands of volts during energetic electron precipitation while a space-walking astronaut would charge to hundreds of

volts. Though the shuttle itself is not at risk at these charging levels, arc discharges are thought to possibly cause dangerous anomalies to the linkage between the orbiter and astronaut. The code that predicted these shuttle charging levels was developed with the aid of actual charging measurements by satellites in polar orbit near 800 kilometers; the focus of this study now turns specifically to these satellites and their charging environment.

CHAPTER III

DEFENSE METEOROLOGICAL SATELLITE PROGRAM

The United States Air Force Defense Meteorological Satellite Program (DMSP) is primarily dedicated to providing tropospheric and near-space environmental data to the military community. Though the principle sensor on DMSP spacecraft produces high resolution visible and infrared imagery of the earth's atmosphere, other instruments measure the *in situ* plasma. The satellites' unique orbits and instrumentation offer an opportunity to study the upper ionosphere at high latitudes.

3.1 Satellite Orbits

The DMSP spacecraft are a series of satellites in circular polar orbits with altitudes near 840 kilometers, orbital inclinations of 98 degrees, and periods of approximately 101 minutes. Two satellites are normally in sun-synchronous orbit at one time; one satellite orbits in the 0600-1800 (dawn to dusk) local time meridian and the other satellite orbits in the 1030-2230 meridian. The four satellites which supplied data for this study are designated as F6 and F8 (0600-1800), and F7 and F9 (1030-2230). The F6 was launched in December, 1982, and was replaced by the F8 in June, 1987, and the F7 was launched in November, 1983, and was replaced by the F9 in February, 1988. With two satellites in different polar orbits at the same time, the high-latitude coverage is appreciable.

Since the geomagnetic and geographic poles are offset, the sun-synchronous DMSP spatial coverage in magnetic local time (MLT) and geomagnetic latitude includes a significant part of the auroral and polar cap regions. Figure 3 illustrates the two satellite combined coverage for northern magnetic latitudes and magnetic local times.
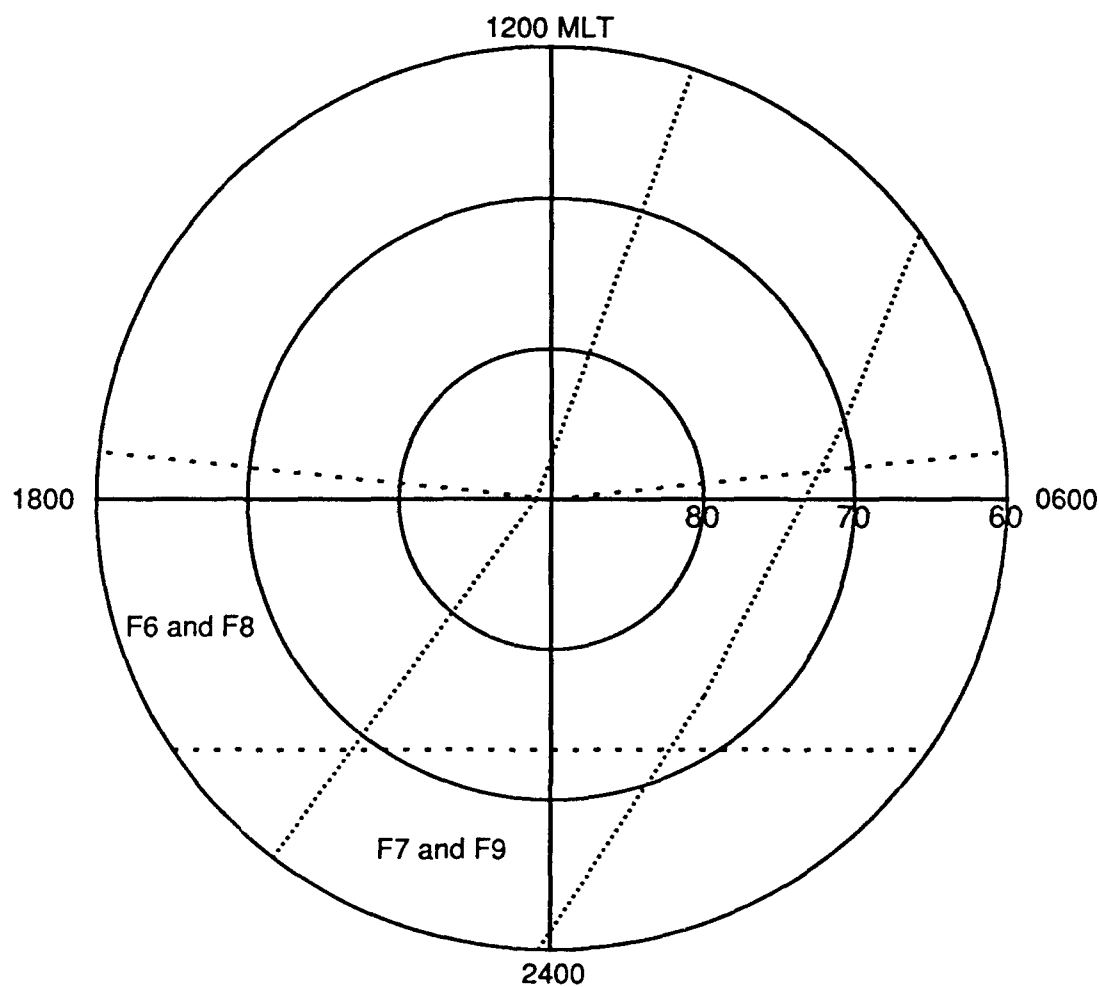
Fig. 3. Orbital coverage of the DMSP F6, F7, F8, and F9 satellites in corrected geomagnetic latitude and magnetic local time over the high-latitude northern hemisphere.

With this extensive high-latitude coverage, spacecraft charging may be studied using the DMSP precipitating electron and ion detector, and a detailed examination of this instrument's operation is necessary to perform subsequent analyses.

3.2 Precipitating Electron and Ion Detector

The precipitating particle detector (SSJ/4) measures the flux of precipitating electrons and ions having energies between 30 eV and 32 keV and identifies the particle spectrum once every second via 20 energy channels. The energy channel configuration of the F8 detector is shown in Table 1 and is generally similar to the F6, F7, and F9 configurations which are shown in Appendix C. A detector consists of four curved plate electrostatic analyzers arranged in two pairs; one pair measures electrons while the second pair measures ions. Each analyzer consists of an aperture system, two curved plates, and a channeltron.

3.2.1 Aperture

The aperture is the opening through which the precipitating particles first pass enroute to being measured. The opening always faces radially outward from the earth, so only precipitating electrons/ions rather than ambient or backscattered particles are measured at high magnetic latitudes. Those charged particles passing through the aperture-defined solid angle then move toward the curved plates and have their energy determined.

3.2.2 Curved Plates

Each electron/ion analyzer has one set of plates with a 60 degree arc of curvature and a second set with a 127 degree arc of curvature. The 60 degree detector measures particles with energies from 32 keV to 1000 eV in channels 1-10 while the 127 degree detector measures particles with energies from 1000 eV to 30 eV in channels 11-20. To identify the flux of particles at these energies, a specific voltage is applied to the plates

TABLE 1. F8 SSJ/4 Energy Channel Configuration

Channel	Central Energy (eV)	Electron Energy Channel Width (eV)	Ion Energy Channel Width (eV)
1	31300	3050	3050
2	21100	2000	2000
3	14300	1330	1330
4	9720	860	860
5	6610	615	615
6	4500	430	430
7	3050	284	284
8	2070	184	184
9	1400	125	125
10	950	88	88
11	950	85	152
12	640	63	102
13	440	42	70
14	310	29	50
15	210	20	34
16	144	13	23
17	98	9.1	16
18	68	6.3	11
19	45	4.2	7.2
20	31	2.9	5.0

for each energy channel, and the resulting electric field between the two plates directs a force toward the inner plate. (The plate polarity of the ion sensor is opposite of the electron sensor). If an incoming particle is one which is meant to be counted in a certain energy channel according to the applied voltage, the electric field will bend the particle's path just enough so that the electron/ion will pass cleanly through the region between the plates and reach the channeltron where it is counted. If the incoming particle's energy is too low, the electric field's force will dominate, and the particle will collide into the inner plate and not be counted. Finally, if the incoming particle's energy is too great, the electric field will be unable to bend the particle's path enough to prevent it from colliding with the outer plate. Such a particle is not normally counted, but high energy particles occasionally scatter through the curved plate region, reach the channeltron, and are inappropriately counted. This is discussed further in section 3.2.5. To make measurements in all 20 energy channels every second, the analyzers' voltages are constantly changing in concert with one another.

The voltage applied across the curved plates steps from high to low through the ten channels of the high energy electron/ion sensors at the same time that it steps through the ten channels of the low energy electron/ion sensors. The voltage for each energy channel is applied constant for 0.098 seconds while 0.002 seconds are used between channel steps to stabilize the changing potential. Sequenced together, the two sets of analyzers return a 20 point electron and ion spectrum once per second. To ensure the analyzers' accuracy and consistency among different satellites, in-flight data coupled with electron and ion beam test results have been used to calibrate the SSJ/4 detectors flown on the F6-F9 satellites.

3.2.3 Calibration

Details of the SSJ/4 calibration are described by *Hardy et al.* [1984] and *Schumaker et al.* [1988]. In summary, the response of the electron sensors was

measured relative to a laser beam's energy and angle with respect to the aperture, and from these measurements an energy-dependent geometric factor, G(E) (cm² ster), was determined. By identifying G (E) at several energies near the central energy of a channel, the response curve for each fixed voltage was determined, and an energy-independent geometric factor, G (cm² ster eV), was calculated by integrating over the response curve such that

$$j(E) = (C/dt)\,(G) \ , \tag{5}$$

where j(E) is the differential flux (particles/cm² sec ster eV) in the channel with central energy E, C is the count level in that channel, and dt is the accumulation interval (0.098 seconds) for these counts. In-flight cross calibration has further enhanced the consistency between one detector's measurements and another's. The ion sensors are identical to the electron sensors (excluding the low energy ion sensor's aperture size) and were assigned geometric factors using a combination of electron beam calibration results, limited ion beam calibration results, and in-flight data. The constants used to convert count rates to fluxes for each of the satellites are shown in Appendix C. The response curve at a fixed voltage also determines the energy range over which a particle may be counted in a specific channel. This value, known as the channel pass band (dE), requires attention when attempting to identify a spacecraft-to-plasma potential difference.

3.2.4 Channel Pass Bands

The SSJ/4 measures precipitating particles between 30 eV and 32 keV via 20 channels with energy steps between channels so large that some particles go undetected. The ratios of the channel pass bands to the central energies range from 8.8 to 9.8 percent for the electron sensors and 8.8 to 16 percent for the ion sensors. The channel pass bands for each F8 channel are shown in Table 1. With a central energy of

310 eV and a dE of 50 eV, the F8 ion channel 14 counts ions with energies from 285 to 335 eV, and with a central energy of 440 eV and a dE of 70 eV, channel 13 counts ions with energies from 405 to 475 eV. Ions with energies from 336 to 405 eV are not counted. Figure 4 depicts the energy ranges over which channels 12 through 19 measure and illustrates the energy gaps between the channels where particles may go undetected. This can make it more difficult to identify charging events since such identification relies on an ion count enhancement from one channel to the next. (The method of identifying charging events is described more fully in section 5.2). However, a fluctuation of the electric potential level during a charging event normally ensures that an ion enhancement will exist in one of the channels (M.S. Gussenhoven, private communication, 1990). Thus, this limitation of the detector is only a minimal concern. Another manageable limitation of the ion detector is electron contamination.

3.2.5 Precipitating Electron Contamination

High fluxes of electrons may cause the ion analyzers' lower energy channels (11-20) to inappropriately record some of the electrons as ions. This occurs because the larger aperture of the low energy ion detector increases the possibility of electron scattering through the curved plates. To quantify this effect, an electron beam system measured the ion channels' responses to various electron energies and determined the ion energy-dependent geometric factor to the electrons ($G_i (E_e)$). Details and resulting factors of this procedure are given in *Schumaker et al.* [1988]. In summary, electron contamination is only significant in ion channels 11 through 20 due to electrons with energies greater than 1 keV and is calculated as follows:

$$\text{Rejected Ion Counts Per Second} = J(E_1) G_i(E_1) (E_1 - E_2) + \sum_{j=2}^{9}$$

$$J(E_j) G_i(E_j) (E_{j-1} - E_{j+1})/2 + J(E_{10}) G_i(E_{10}) (E_9 - E_{10}) , \tag{6}$$
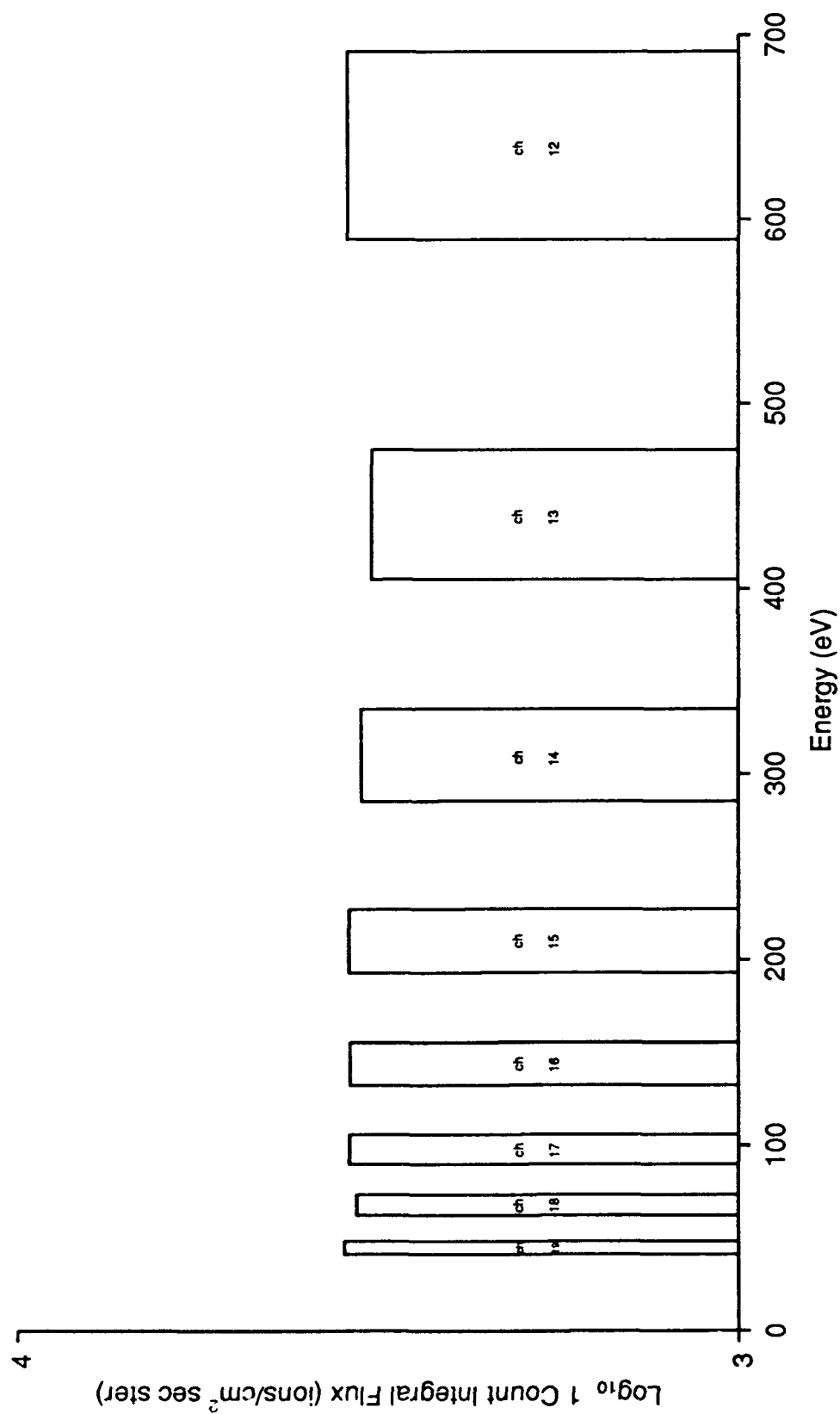
Fig. 4. Channel pass bands (channels 19 through 12) for the DMSP F8 SSJ/4 ion detector.

where $J(E_j)$ is the differential number flux of precipitating electrons of energy E in channel j described by equation (5), and $G_i(E_j)$ is the ion channel energy-dependent geometric factor to electrons of energy E_j. The actual ion count in a channel is the reported count minus the rejected count. The practical result of this correction is to erase or fine tune a measured ion spectrum. While the SSJ/4 sensors measure electron and ion precipitation, another instrument determines the ambient plasma density.

3.3 Thermal Plasma Detector

The Special Sensor for Ions, Electrons, and Scintillation (SSIES) on the F8 and F9 satellites measures the ambient plasma density. Though a similar instrument flew on the F6 and F7, it was inoperable during the period of this study (F.J. Rich, private communication, 1990). The sensor consists of a planar ion-retarding potential analyzer to determine the densities of different ion species, a planar total-ion-density trap or scintillation meter to measure the total ambient ion density and its fluctuations, a planar ion-drift meter to measure the bulk flow velocity of the thermal plasma, and a spherical Langmuir probe to measure the ambient electrons. A detailed description of the instrument is given by *Greenspan et al.* [1986]. The F8 and F9 ambient plasma density measurements for the period of this study were available only from the scintillation meter (F.J. Rich, private communication, 1990).

The ion scintillation meter (SM) is mounted in a common ground plane with the retarding potential analyzer and has a circular aperture and collecting plate facing the ram direction. Sensors keep the reference potential at the aperture close to the plasma potential. The SM uses no retarding voltage, so all ions falling through the aperture are measured, and thermal electrons are electrostatically blocked from reaching the collector plate. However, extreme precipitating electron fluxes may contaminate the SM measurements, but no formula exists which computes the level of contamination; thus, the measured density just before and after the most intense electron precipitation may

best characterize the thermal plasma environment (F.J. Rich, private communication, 1991). The ion density is reported once per second and is a function of the current collected and the spacecraft's velocity, and these measurements are used in the analysis of Chapter V. An earlier investigation of DMSP spacecraft charging used similar ambient plasma measurements together with precipitating particle data to characterize the charging environment, and the results of that study are now presented.

CHAPTER IV

PREVIOUS STUDY OF DMSP CHARGING

Gussenhoven et al. [1985] performed a partial survey of DMSP F6 and F7 precipitating particle measurements taken during January, November, and December, 1983, and identified eleven negative charging events ≥ 47 volts. The electric potential between the vehicle and local plasma exceeded -100 volts only when the satellite encountered intense energetic electron precipitation while in a region of locally depleted thermal plasma density within the earth's shadow. A positive correlation was found between the charging magnitudes and the ratio of the high energy (≥ 14 keV) electron integral number f to the ambient plasma density. The study's results are presented as a quantitativ f ndation for the low-earth polar orbit charging environment.

4.1 Charging Results

A summary of the charging events reported by *Gussenhoven et al.* [1985] is shown in Table 2. Peak charging magnitudes vary from -47 to -679 volts, and the charging events last 2 to 62 seconds. In all cases, the total electron integral number flux is near or greater than 10^9 electrons/(cm^2 sec ster) while the integral number flux due to electrons ≥ 14 keV ranges from 10^7-10^{10} electrons/(cm^2 sec ster). As described in section 2.3, higher energy electrons normally contribute more to a significant surface charge imbalance.

4.1.1 Electron Fluxes

For those charging events listed in Table 2, the total electron integral number fluxes do not correlate as well as the higher energy electron integral number fluxes do to the charging magnitudes. As an example of the relationship between high energy

TABLE 2. Summary of Charging Events Reported by *Gussenhoven et al.* [1985]

Day	UT (sec.)	Satellite	Φ_{max} (-volts)	ΔT (sec.)	Log_{10} Electron Fluxes (electrons/cm^2 sec ster) Total	$\geq$14keV	Log_{10} Ambient Plasma Density (cm^{-3})	Log_{10} Ion flux (ions/cm^2 sec ster)
1/6/83	49,480	F6	213	24	9.16	8.08	3.41	6.49
1/10/83	74,722	F6	68	12	9.58	7.32	4.13	6.59
1/12/83	35,877	F6	462	17	10.01	9.97	2.73	7.66
1/20/83	50,047	F6	679	3	10.77	9.80	2.54	5.95
1/21/83	54,937	F6	100	12	9.26	9.17	---	5.72
11/26/83	47,712	F6	317	18	10.12	9.66	----	8.25
11/26/83	66,068	F6	462	16	9.22	7.68	----	6.34
11/26/83	43,841	F7	47	4	8.90	7.68	3.13	7.25
11/26/83	49,843	F7	314	60	9.20	9.06	2.10	8.32
12/1/83	1,458	F7	215	2	9.37	9.29	3.55	7.48
12/31/83	14,007	F7	462	62	9.38	9.35	1.09	8.17

electron fluxes and charging, Figure 5 depicts the total electron integral number flux, the electron integral number flux due to electrons with energies between 14 keV and 30 keV, and the DMSP F6 satellite potential as a function of time during one of the charging events on November 26, 1983. The satellite potential is poorly related to the total electron flux and is more closely related to the higher energy electron flux. The peak potentials of -317 volts coincide with fluxes due to electrons ≥ 14 keV exceeding 10^9 electrons/(cm^2 sec ster). While the largest total electron flux in Figure 5 is greater than 10^{10} electrons/(cm^2 sec ster) at 47700 seconds UT, the ≥ 14 keV electron flux is at or below 3×10^7 electrons/(cm^2 sec ster), and spacecraft charging does not occur. Relationships between charging and high energy electron fluxes other than ≥ 14 keV were not reported, so the ≥ 14 keV relationship should be considered only as a general indication of which electrons may be causing the charging rather than as defining a key threshold. *Gussenhoven et al.* [1985] also found that thermal plasma densities influence DMSP charging.

4.1.2 Ambient Plasma Densities

The thermal plasma densities for the charging events in Table 2 range over three orders of magnitude and are primarily well below 10^4 cm^{-3}. As discussed in section 2.3.1, the ambient ions are a current source which can neutralize negative charge imbalances caused by other currents. Though a positive correlation exists between higher magnitude charging events and lower plasma densities, *Gussenhoven et al.* [1985] found a better correlation between the charging levels and the ratio of the ≥ 14 keV flux to the ambient plasma density. As already mentioned, 14 keV is not necessarily a key electron energy, but a study of the electron fluxes that resulted in these charging events suggests that the electron spectra may be categorized.
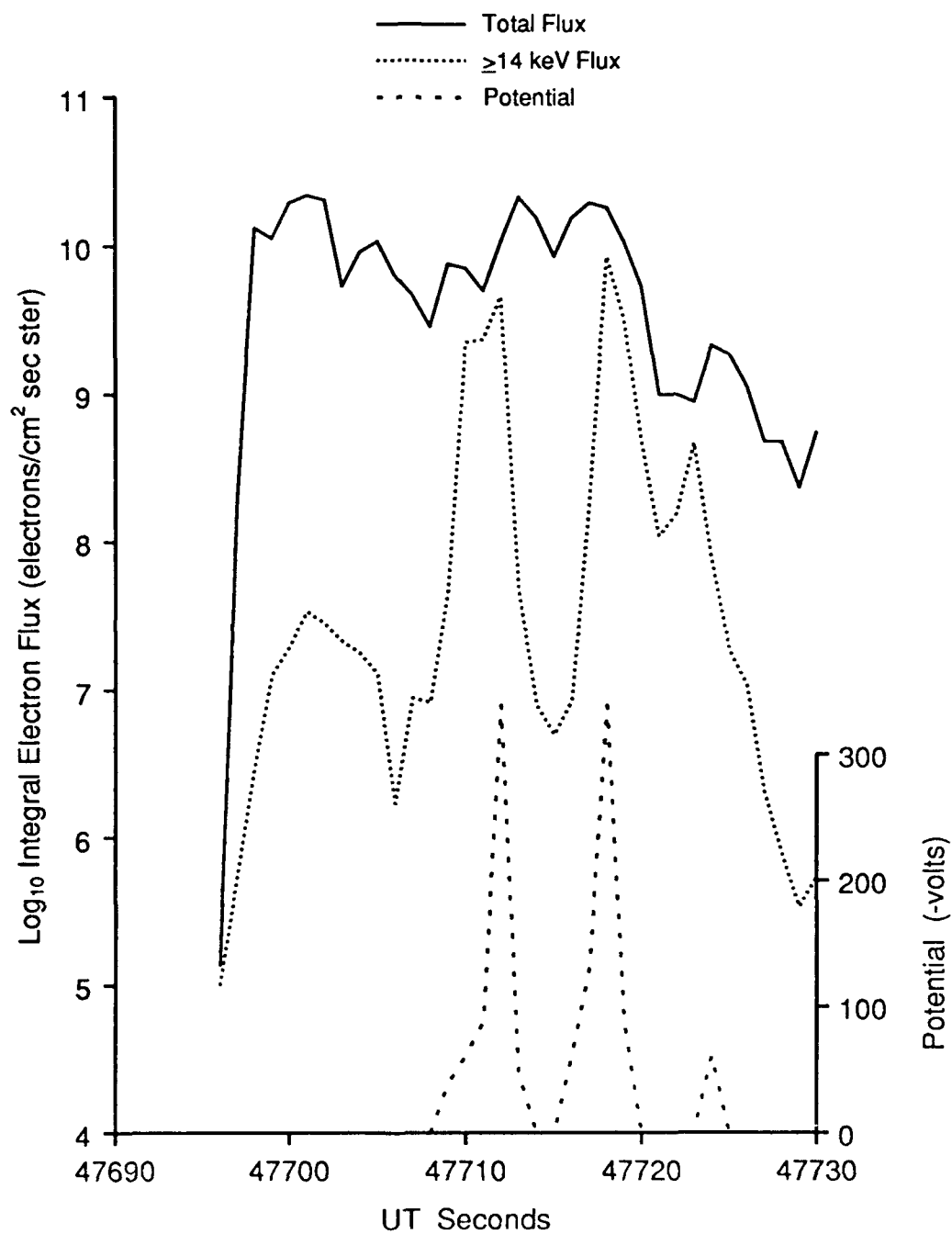
Fig. 5. The electron integral number flux for the SSJ/4 total energy range (solid line) and for energies ≥14 keV (dotted line), and the DMSP F6 satellite potential during a charging event on November 26, 1983 (after *Gussenhoven et al.*, 1985).

4.2 Model Electron Spectral Characteristics

4.2.1 Spectral Types

Yeh and Gussenhoven [1987] evaluated the higher energy (≥ 1 keV) precipitating electron profiles that resulted in the DMSP charging events reported by *Gussenhoven et al.* [1985] and classified 92% of the spectra into four groups in an attempt to model the precipitating spectra. Figure 6 depicts the measured log distribution function versus energy for the four types of electron spectra. Type 1 is a two-Maxwellian distribution function in which electrons below 12 keV carry most of the flux. Type 2 is a nearly constant distribution function up to an energy near 17 keV and then becomes Maxwellian at higher energies. Type 3 resembles an inverted-V spectrum [*Frank and Ackerson,* 1971; *Lin and Hoffman,* 1979] with a peak near 17 keV and a Maxwellian fit at higher energies, and type 4 is primarily an increasing distribution function out to 30 keV with unknown characteristics at higher energies. The one second electron spectra are grouped in Table 3 for seven levels of charging. While the majority of the charging levels for types 1, 2, and 3 are less severe than -100 volts, the negative potentials for all but one of the type 4 events meet or exceed 100 volts and are a probable result of the increased fluxes of higher energy electrons carrying the greatest charging current. The average integral fluxes for each spectral type help characterize these populations.

4.2.2 Electron Fluxes

Yeh and Gussenhoven [1987] calculated the average electron integral fluxes of spectral types 1-3. As shown in Table 3, the total number flux of type 1 is near 10^{10} electrons/(cm^2 sec ster), and over 96% of this flux is due to electrons below 12 keV. The total number flux of type 2 is slightly more than half of that of type 1, but 36% of the number flux of type 2 is due to electrons ≥ 17 keV. Assuming that higher level charging occurs with higher energy ctron precipitation, the type 2 spectra are more
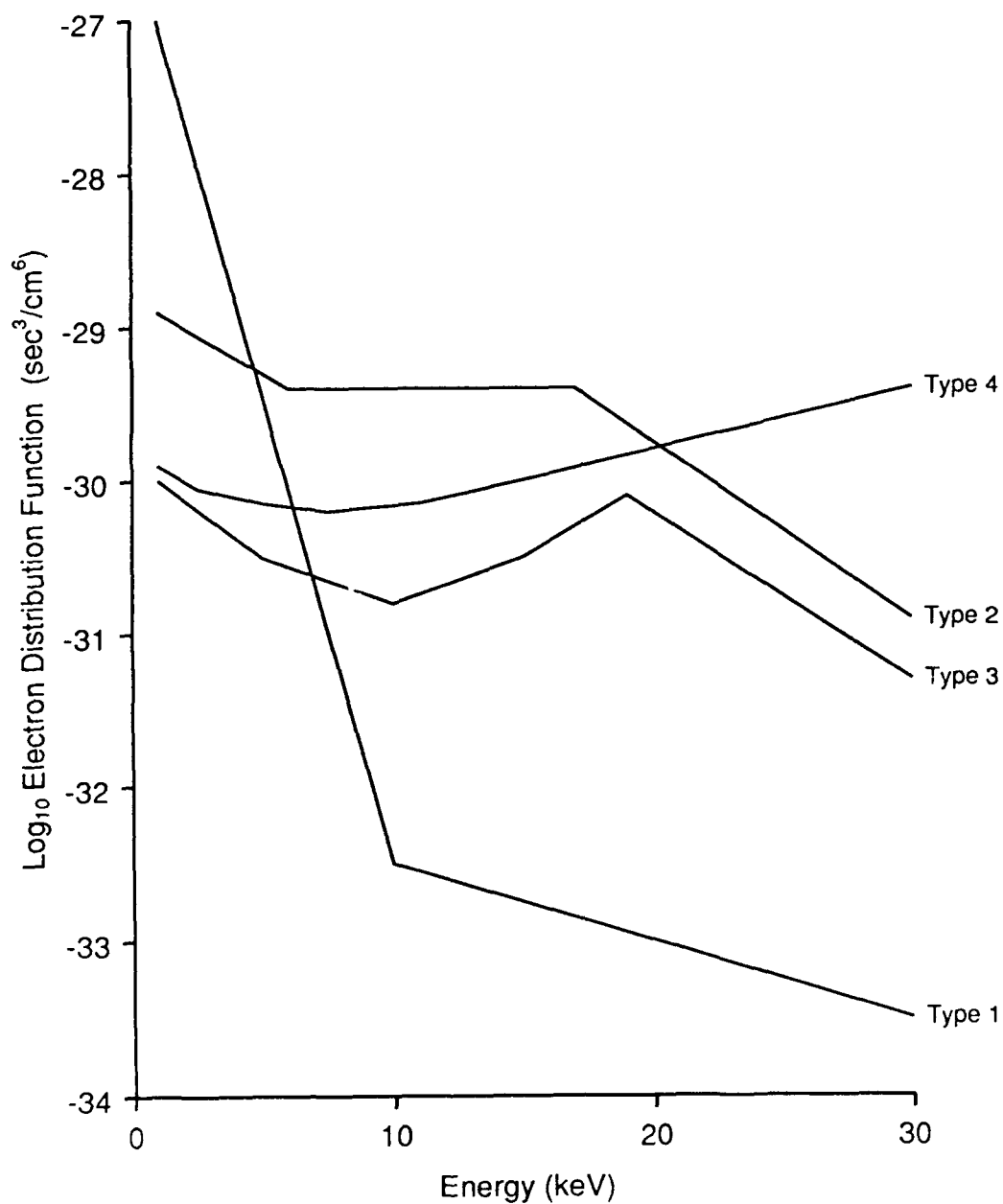
Fig. 6. Four spectral types of precipitating kiloelectronvolt electrons during DMSP charging events reported by *Gussenhoven et al.* [1985] (after *Yeh and Gussenhoven*, 1987).

TABLE 3. Charging Electron Spectra Characteristics (after *Yeh and Gussenhoven*, 1987)

Potential (-volts)	Type 1	Type 2	Type 3	Type 4	Not Grouped
< 100	13	50	56	1	10
100	3	18	7	5	3
145	2	8	8	1	1
213-215	1	4	1	2	0
314-317	1	3	2	0	0
462	0	0	0	2	1
679	0	1	0	0	0
Total	20	84	74	11	15
Percentage	9.8%	41.2%	36.3%	5.4%	7.4%
Avg. Total Flux (electrons/ cm^2 sec ster)	1×10^{10}	5.7×10^9	2.3×10^9	-----	-----
Avg. ≤ 12 keV Flux (electrons/ cm^2 sec ster)	9.7×10^{10}	-----	-----	-----	-----
Avg. ≥ 17 keV Flux (electrons/ cm^2 sec ster)	----	2×10^9	1×10^9	-----	-----

likely to cause significant charging than type 1 as the results suggest. The total number flux of type 3 is less than 25% of type 1, but like type 2, a large part (45%) of this total is due to electrons near and above 17 keV. The primary spectral difference between types 2 and 3 is at energies below 17 keV where the less energetic electrons are less intense in type 3. This becomes important when considering the difference in secondary electron productions [*Katz et al.*, 1986].

4.2.3 Models of DMSP Charging

Primary electrons and their backscattered and secondary electron productions together with ambient plasma densities provide the framework for the modeling efforts of *Yeh and Gussenhoven* [1987]. Results of their models show positive correlations between negative potential levels and the ratio of the electron number flux above some model energy (E_c) (unique to each electron spectral type) to the ambient plasma density. Their models are limited by unique spectral types (which were based on 11 charging events), and both E_c and the electrons fluxes above E_c necessary to produce charging vary significantly depending on the backscattered and secondary coefficients used. Also, the model spectra do not include electrons below 1 keV, so a key source of secondary electrons is not considered. While interpreting the electron spectra described here is not difficult, some ambiguity may exist as briefly noted in section 3.2.4 in determining whether the corresponding ion spectra represent satellite charging. Thus, a brief summary of the ion spectra reported by *Gussenhoven et al.* [1985] is presented.

4.3 Charging Identification

The method *Gussenhoven et al.* [1985] used to identify charging events mirrors that of *DeForest* [1972] and is explained in detail in section 5.2. Simply stated, an enhanced flux of positive ions toward a satellite can be due to a significant negative charge imbalance on the spacecraft's surface which attracts the ions and, therefore, may

represent spacecraft charging. The ion fluxes in the charging channel for the charging cases in Table 2 range from 8.8×10^5 to 2.07×10^8 ions/(cm^2 sec ster) and are at least one order of magnitude less than the total electron number flux. Detailed information on the ion spectra was provided only for the charging event with the greatest ion flux (November 26, 49,843 seconds UT), and the respective ion counts and distribution function for this exceptional case are shown in Figure 7. The ion count in the charging channel (channel 14) is nearly three orders of magnitude greater than the preceding channel count and illustrates the sudden change in ion flux from one channel to the next during a charging event. While ion distribution data was not reported for the other charging cases, the size of the ion enhancement shown in Figure 7 should not be considered the norm. Moreover, the temporal nature of the charging environment and the limitations of the instrument, particularly the channel pass bands discussed in section 3.2.4, preclude such extraordinary measured ion fluxes as being necessary to conclude the presence of spacecraft charging. Finally, though the study by *Gussenhoven et al.* [1985] did not focus on solar cycle influences of DMSP charging, the relationship found between ambient plasma density and satellite charging suggests a possible solar cycle dependence since the solar EUV energy contributes largely to the plasma density.

4.4 Solar Cycle Phase

To illustrate the solar cycle phase during *Gussenhoven's et al.* [1985] study, the 10.7 cm solar fluxes for January, November, and December, 1983, are shown in Figure 8 with arrows denoting the charging days. January is represented by a relatively moderate flux between the 1981 maximum and the 1986 minimum while November and December 1983 fluxes have dropped toward the 1986 minimum. Based solely on these 10.7 cm fluxes and assuming plasma densities near 800 kilometers are lower during periods of lower solar flux, charging may be expected to be more frequent or intense

Channel	Central Energy (eV)	Ion Counts
20	32	50
19	47	83
18	69	112
17	100	145
16	147	221
15	215	353
14	314	108455
13	462	1226
12	679	118
11	995	91
10	985	1
9	1430	1
8	2100	1
7	3050	1
6	4470	1
5	6570	1
4	9570	2
3	14070	1
2	20710	1
1	30340	1
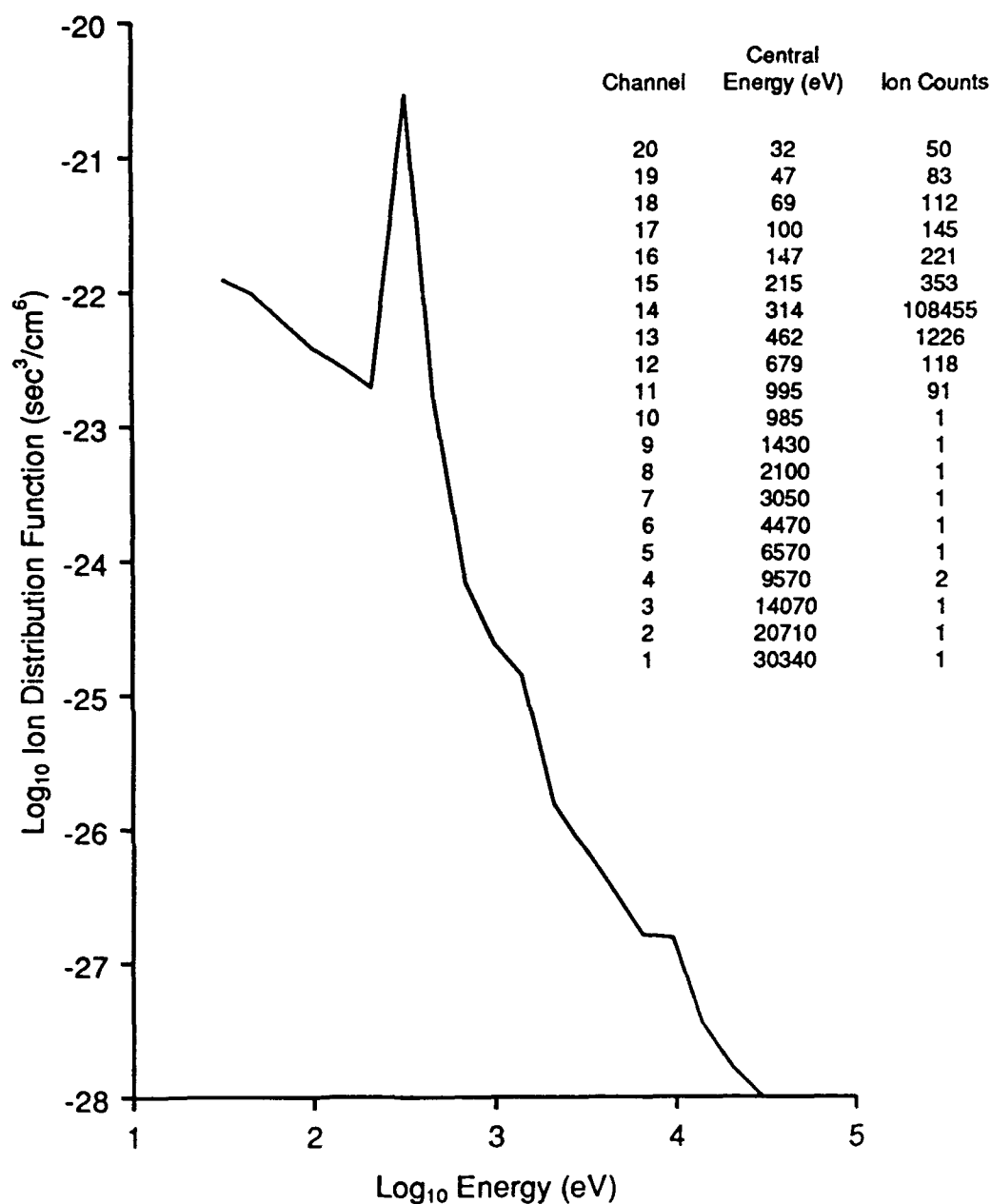
Fig. 7. Ion distribution function during -314 volt charging event on November 26, 1983, and ion counts in each of the F7's SSJ/4 energy channels (after *Gussenhoven et al.*, 1985).
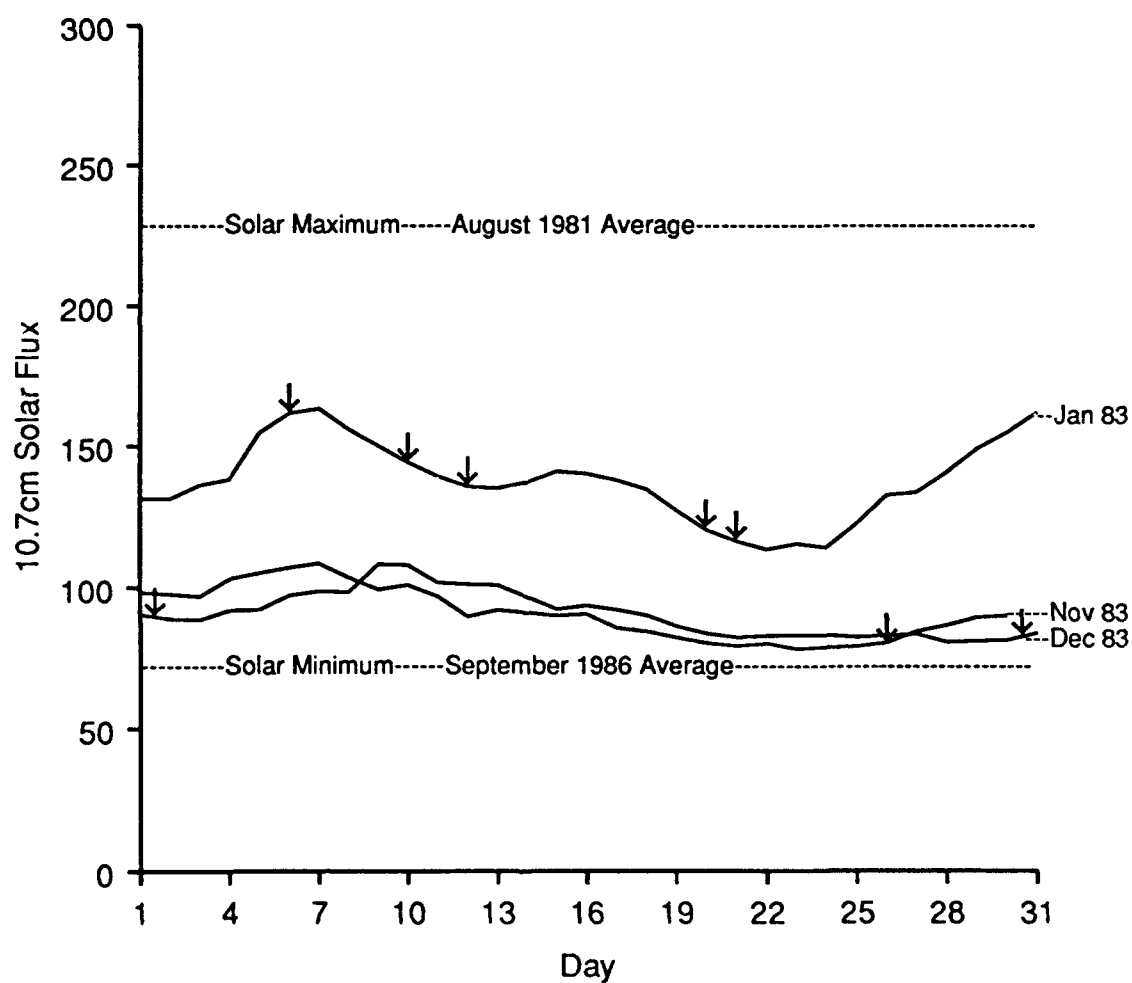
Fig. 8. Solar flux levels (10.7 cm) during January, November, and December of 1983 with arrows denoting days of DMSP charging.

during November or December rather than January. This was not the result reported by *Gussenhoven et al.* [1985]. However, since the frequency and intensity of energetic electron precipitation (a key source of spacecraft charging) were not specifically considered, a conclusion concerning the solar cycle cannot be based on these results alone. Furthermore, their survey of F6 and F7 data did not include an extensive search for every charging event. In contrast, this investigation of DMSP charging is exhaustive in identifying all charging events during winter periods of solar maximum and solar minimum, and that of the former is now presented.

CHAPTER V

DMSP CHARGING -- SOLAR MAXIMUM

This part of the investigation aims to characterize the general state of spacecraft charging within the high-latitude upper ionosphere during solar maximum conditions and to identify the environmental parameters controlling the charging conditions. Before the study's results are presented, a description of the data base and analysis procedures is given.

5.1 Data Base

The data base consists of SSJ/4 precipitating particle measurements taken poleward of 50 degrees north magnetic latitude by the DMSP F8 satellite during November and December, 1989, and January, 1990, and by the F9 satellite during December, 1989, and January, 1990. Select SSIES ambient plasma density data from this period is also included. These winter months were chosen because they coincide with extended periods of eclipsed flight to minimize photoemission and were believed to provide high-latitude ionospheric conditions more conducive to spacecraft charging (lower ambient plasma densities). The 10.7 cm solar fluxes and 3 hour Kp sums during this solar maximum period are shown in Figure 9 in contrast to those during 1986-87. The satellites reported SSJ/4 data more than 90 percent of the time and generated 2.8 million electron/ion spectra. By applying a fundamental electrostatic principle (Liouville's Theorem), the ion spectra were used to identify spacecraft-to-plasma potential differences.

5.2 Charging Identification Theory

When an electric potential difference exists between a negatively charged object in
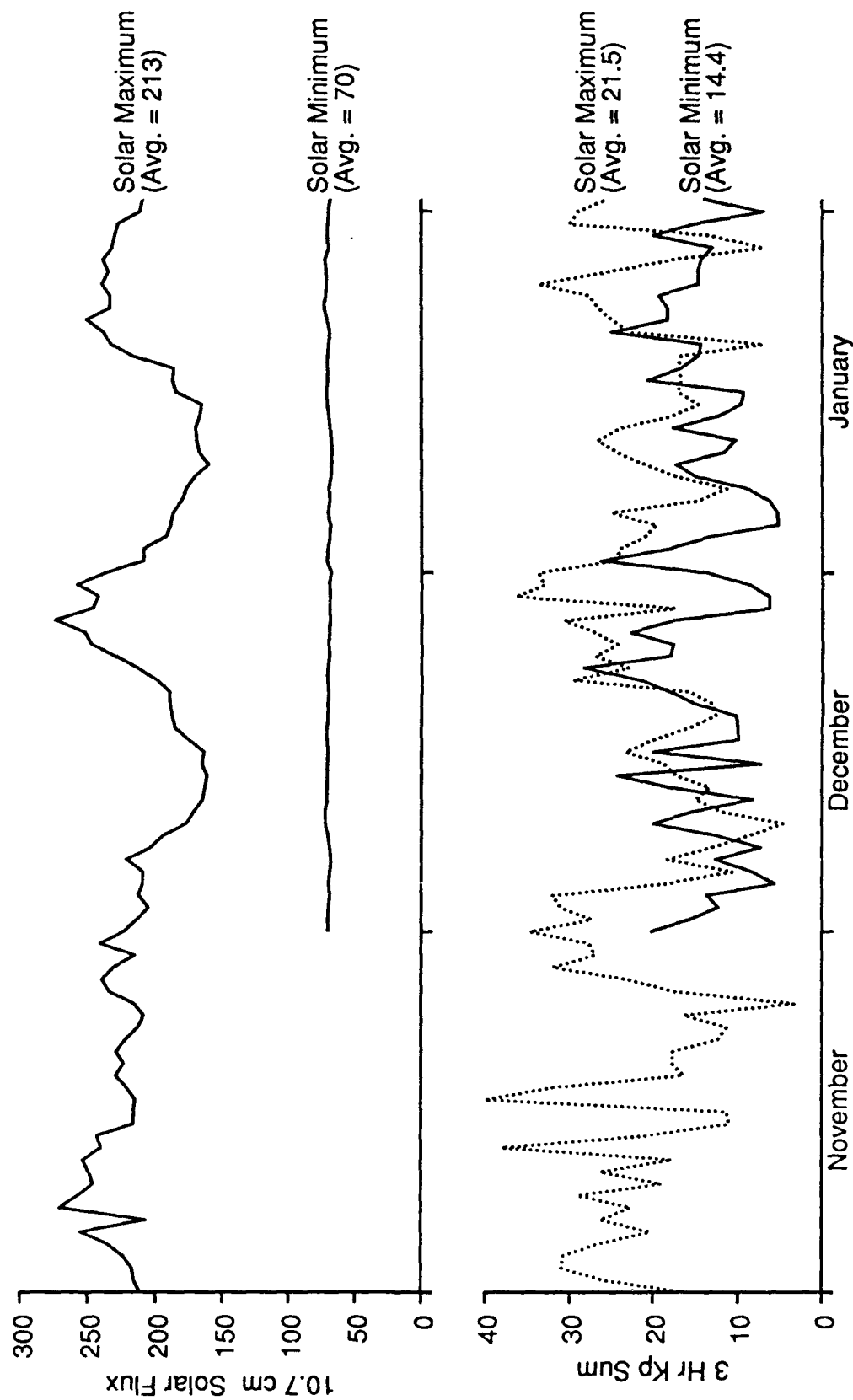
Fig. 9. Solar 10.7 cm flux levels (top) and 3 hour Kp sums (bottom) during winter periods of solar maximum (1989-90) and solar minimum (1986-87).

space and the surrounding plasma, the corresponding electric field directs a force on a positive ion toward the charged object. As the ion accelerates, its energy change (ΔU) from one point to the next is equal to its charge (q) times the difference in potential between the two points ($\phi_2 - \phi_1$); $\Delta U = q\Delta\phi$. If ΔU and q are known, $\Delta\phi$ is easily calculated. Since the energy of ambient ions is relatively small in LEO (≤ 0.1 eV), then the energy of a singly charged ambient ion reaching a charged spacecraft closely approximates ΔU and, therefore, reflects the potential difference between the vehicle and plasma. For a given negative potential, all ions reaching the satellite must have energies equal to or above $-q\phi$ since they are accelerated through the potential before being measured; thus, counts of ions at lower energies are negligible. The lack of ion counts in the lower energy channels and a sudden flux enhancement in the charging channel result in a unique ion spectrum. This method of identifying spacecraft charging is well accepted, has been used in other experiments [*DeForest*, 1972; *Mullen and Gussenhoven*, 1982; *Gussenhoven et al.*, 1985], and is the principle technique used in this study.

5.3 Experimental Methods

5.3.1 Search for Charging Events

Nearly 3 million ion spectra of the solar maximum data base were examined for charging profiles. A computer program encoded with the principles just described sorted the ion spectra and selected possible charging events. Ion signatures due to other phenomenon such as ion precipitation in a narrow energy band often resemble a charging profile, and rapidly changing potential levels can yield less bold charging signatures as mentioned in section 4.3. Therefore, to ensure not to miss genuine charging events, the computer code selected all charging-like ion distributions, and then each of these spectra was examined in detail. Ion precipitation and SSJ/4 anomalous

values created some challenge in selecting only real charging events.

5.3.2 Ion Spectral Analysis

Ion precipitation and actual vehicle charging events have unique ion spectral characteristics which allow for proper classification. While ion precipitation of magnetospheric origin possesses multiple distributions, the ions' energies and number fluxes are likely to be ordered from one second to the next, and the same is true of the satellite's measurements as it orbits through a region of ion precipitation. In contrast, the ions' energies and number fluxes associated with a charging event should be more unordered as the charging levels change constantly and the SSJ/4 sweeps through 20 energy channels every second (D.A. Hardy, private communication, 1990). Moreover, though at any one moment the charging and precipitating ion spectra may be similar, the distributions before and after the spectra in question reflect the nature of the environment.

A change of the peak ion flux from one channel to the next is somewhat random during actual charging while ion counts during ion precipitation change more gradually from one channel to the next. This is a key characteristic used to distinguish ion precipitation. Also, a charge (current) imbalance as described in Chapter II is necessary to create spacecraft charging, and only energetic electron precipitation can normally generate significant negative potentials. Thus, the presence or absence of high energy electron precipitation further aids the identification process though the SSJ/4's inability to measure particles above 32 keV must also be considered. Ion precipitation and SSJ/4 anomalous readings were sorted by collectively using these selection tools, and this process resulted in thousands of ion spectra being discounted as representing satellite charging. Finally, to better understand spacecraft charging during solar maximum conditions, the data analysis included examining periods of energetic electron fluxes in

which charging did not occur.

5.3.3 Precipitating Electron and Ambient Plasma Analysis

Based on the charging environment reported by *Gussenhoven et al.* [1985] and *Yeh and Gussenhoven* [1987], all periods for which ≥ 9.7 keV electron fluxes exceeded 3×10^8 (electrons/cm^2 sec ster) measured by the SSJ/4 were selected for analysis and compared to those during solar minimum. The frequency of intense energetic electron precipitation was studied together with ambient plasma densities measured by the SSIES. This analysis, coupled with a thorough search for genuine charging cases, completed the study of DMSP spacecraft charging during solar maximum, and the results are now presented.

5.4 Solar Maximum Charging Results

Significant spacecraft charging was absent during solar maximum conditions. A DMSP satellite charged to -45 volts only one time, and this relatively weak potential lasted just two seconds. The environment which generated this single charging event is examined and compared to a similar environment which did not cause charging. The frequency of energetic electron precipitation during the period of study is then quantified, and the measured ambient plasma densities within regions of electron precipitation are identified.

5.4.1 Analysis of Charging Event

The single charging event during solar maximum is summarized in Table 4. Nearly half of the total precipitating electron integral number flux is due to electrons ≥ 3 keV while electrons ≥ 9.7 keV contribute over 17 percent; these features are consistent with the theory and experimental results discussed in Chapters II and IV though the

TABLE 4. Summary of Charging Event During Solar Maximum

Date: November 13, 1989

Time: 2231:50 - 2231:51 UT

Satellite: F8

Magnetic Latitude: 67° N *

Magnetic Local Time: 0450 *

Peak Potential: -45 volts

Total Electron Integral Flux: 2.7×10^{10} electrons/(cm^2 sec ster)

≥ 3.0 keV Electron Integral Flux: 1.2×10^{10} electrons/(cm^2 sec ster)

≥ 9.7 keV Electron Integral Flux: 4.8×10^{9} electrons/(cm^2 sec ster)

Ambient Plasma Density: 2.0×10^{4} cm^{-3} **

Ion Integral Flux in Charging channel: 6.35×10^{7} ions/(cm^2 sec ster)

---

* The satellite is just out of eclipse though the SSJ/4 remains in shadow.

** Value is approximate as electron fluxes affect scintillation meter output.

electron spectrum does not closely fit any of the particular spectral types of *Yeh and Gussenhoven* [1987]. The electron and ion distributions during the event are shown in Figure 10. The electron distribution represents the fifth largest number flux of electrons ≥ 3 keV in the entire solar maximum data base, and the enhanced flux of 45 eV ions depicted in the ion distribution signals a -45 volt spacecraft-to-plasma potential difference. The thermal plasma density of 2.0×10^4 cm^{-3}, though greater than all of the densities during the charging events reported by *Gussenhoven et al.* [1985], represents one of the lower plasma densities identified in this study during solar maximum periods of enhanced energetic electron precipitation. The sole charging event during solar maximum is the result of one of the more energetic electron distributions combining with a relatively low plasma density. Only on two other occasions were the electron fluxes more energetic and the thermal plasma less dense.

5.4.2 Analysis of Non-Charging Event

The lowest plasma density recorded when ≥ 3 keV electron fluxes surpassed $10^{9.5}$ electrons/(cm^2 sec ster) while in shadow was 1.3×10^4 cm^{-3} at 1429:31 UT on January 15, 1990. At the same time, the high energy tail of the precipitating electron distribution was greater than that during the -45 volt charging event. The greater energetic electron flux coupled with the decreased density seems to suggest that a similar or more extreme potential difference might form. However, detectable charging did not occur. Figure 11 depicts the electron distributions of the charging and non-charging cases and shows that the low energy tail of the F9 electron distribution is also significantly larger than that of the F8 charging case. The increased number of secondary electrons generated by the lower energy precipitating electrons as discussed in section 2.3.3 may explain the lack of charging. The second instance of a lower plasma density coupled with a greater high energy electron flux exhibited an electron distribution similar to that of the F9 on January 15. Since charging was all but absent during solar maximum conditions, the
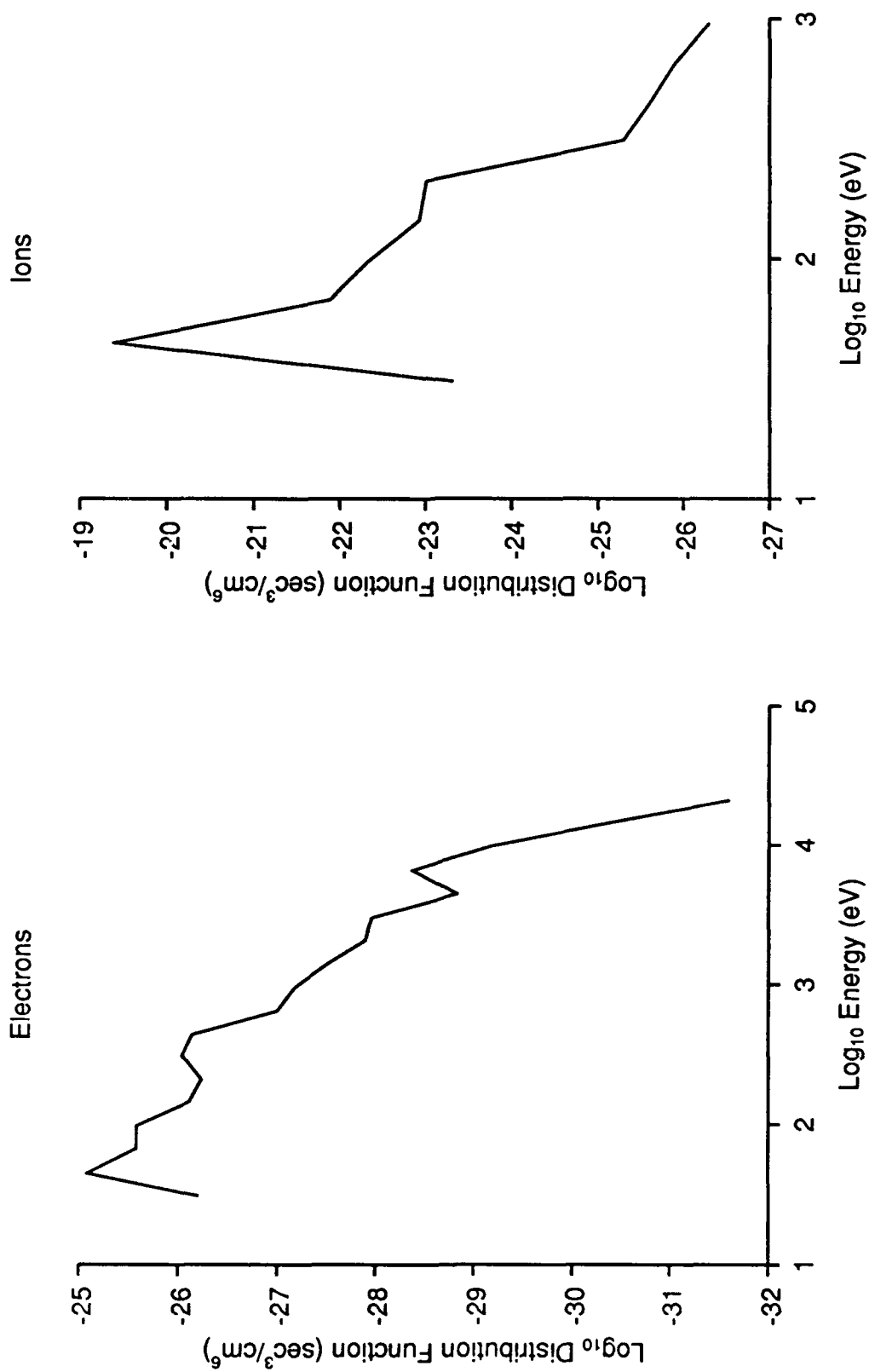
Fig. 10. Distribution functions for electrons (left) and ions (right) during -45 volt charging event on November 13, 1989.

45
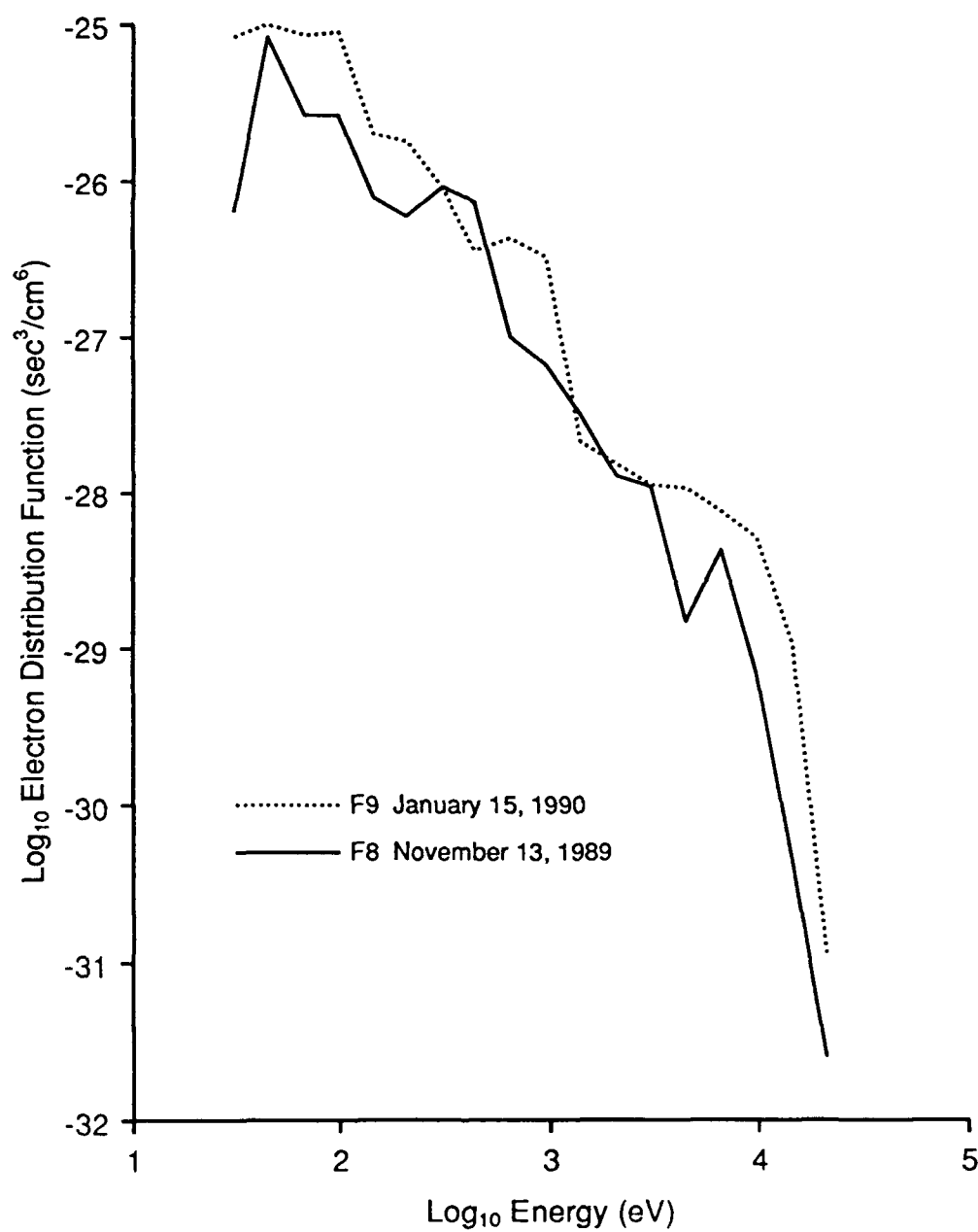
Fig. 11. Electron distribution function during -45 volt charging event in relation to a greater electron distribution which did not generate charging.

frequency of the primary charging current (energetic electron precipitation) along with the thermal plasma densities measured during this precipitation must be considered.

5.4.3 Frequency of Energetic Electron Precipitation

The total number of seconds that the F8 and F9 satellites encountered intense energetic electron precipitation is shown in Table 5. Also listed in Table 6 is the total time that the satellites encountered intense electron precipitation of lesser energy. These values characterize the frequency of electron precipitation and may be compared to those during solar minimum given in section 6.3.9. In summary, based solely on the electron distributions during the charging events reported by *Gussenhoven et al.* [1985], the electron precipitation during solar maximum conditions was energetic enough and encountered often enough to generate numerous charging events. Since charging did not occur, the ambient plasma densities which accompanied the electron precipitation must be examined.

5.4.4 Measured Ambient Plasma Densities

With two exceptions, measured thermal plasma densities ranged from 1.3×10^4 cm^{-3} to 1.3×10^5 cm^{-3} during periods of enhanced electron precipitation within the earth's shadow. The precipitating electron distributions during several of these periods resemble those of *Gussenhoven et al.* [1985] for which charging did occur. In comparing specific cases, the only significant difference between the two environments is in the thermal plasma density; the densities are one to three orders of magnitude greater during solar maximum. During solar minimum, ambient plasma densities are likely to be lower, and a study of spacecraft charging during solar minimum may provide contrasting results.

TABLE 5. Frequency (seconds) of ≥ 9.7 keV Electron Fluxes Greater than $10^{8.5}$ (electrons/cm^2 sec ster) During Solar Maximum

Satellite	F8	F9
November 1989	410 (.07%)	----
December 1989	530 (.09%)	703 (.12%)
January 1990	415 (.08%)	534 (.10%)

Values in parentheses represent the percentage of the total time that the satellites encountered these fluxes poleward of 50° N magnetic latitude.

TABLE 6. Frequency (seconds) of Total Electron Fluxes Greater than $10^{9.3}$ (electrons/cm^2 sec ster) During Solar Maximum

Satellite	F8	F9
November 1989	1306 (.23%)	----
December 1989	1745 (.30%)	3204 (.56%)
January 1990	1485 (.28%)	2753 (.51%)

Values in parentheses represent the percentage of the total time that the satellites encountered these fluxes poleward of 50° N magnetic latitude.

CHAPTER VI

DMSP CHARGING -- SOLAR MINIMUM

This portion of the study seeks to characterize the general state of high-latitude LEO spacecraft charging during solar minimum conditions and to illustrate the parameters responsible for the presence or absence of charging. After the data base is identified, the study's methodology is reviewed, an additional analysis tool is introduced, and the results are presented.

6.1 Data Base

The solar minimum data base is similar in location and month to that of solar maximum and consists of SSJ/4 measurements taken poleward of 50 degrees north magnetic latitude by the F6 and F7 satellites during December, 1986, and January, 1987. The 10.7 cm solar fluxes and 3 hour Kp sums during this period may be compared to those of solar maximum in Figure 9 of Chapter V. The near constant solar flux during solar minimum differs sharply from the pronounced fluctuations during solar maximum. A thorough search through the data base's 2.3 million ion spectra was performed to identify all charging events.

6.2 Experimental Methods

The electromagnetic principles, computer codes, and methods outlined in Chapter V were also used to analyze the solar minimum data. The only procedural difference concerns the ambient plasma densities; measured ambient plasma data for the F6 or F7 is not available for periods after January, 1984. Instead, the Time Dependent Ionospheric Model (TDIM) is used to characterize the thermal plasma environment.

The TDIM is a global scale, three-dimensional, and time-dependent computer model which numerically solves the continuity, momentum, and energy equations for ions and the energy equation for electrons between 120 and 800 kilometers. The model considers several processes such as plasma production due to direct and scattered EUV radiation and high-latitude precipitation, diffusion, chemical reactions, winds, electrodynamic interactions, and further takes into account the offset between the geomagnetic and geographic poles. A detailed description of the TDIM and several model-to-observation comparisons are given in a review by *Sojka* [1989], and a mathematical presentation of the TDIM's methodology is given by *Schunk* [1988]. Though DMSP spacecraft orbit nearly 40 kilometers above the model's upper boundary, significant ambient plasma density gradients between 800 and 840 kilometers are not normally present because of large plasma scale heights at these altitudes. Thus, the TDIM's output for 800 kilometers predicts the ambient plasma densities encountered by the satellites and provides key input in analyzing the results of solar minimum charging.

6.3 Solar Minimum Charging Results

Significant spacecraft-to-plasma negative potential differences occurred often during solar minimum conditions. In great contrast to that during solar maximum, DMSP satellites charged negatively on 169 occasions with peak potentials ranging from -45 volts to -1.4 kilovolts. A summary of the events is presented first, and a plot of magnetic latitudes and local times reflects a common region for most of the charging cases. The electron population responsible for various charging levels is then examined, and two charging events more severe than ever reported for the DMSP are identified. The time constant for the satellites' potential to react to electron flux changes is considered, and model thermal plasma densities are presented for various conditions and locations. Finally, the frequency of enhanced energetic electron fluxes is compared to

that of solar maximum, and a relationship between charging events and the Kp index is investigated.

6.3.1 Charging Summary

The 169 negative charging events during solar minimum are listed in Appendix A, and a summary of the events' magnitudes and durations are shown in Figure 12. The charging levels shown represent the greatest potential achieved during the entire event and are defined as the central energy of the SSJ/4 channel measuring the enhanced ion flux. Durations shown represent a presence of any negative charging level ≥46 volts. A complete time history of select events is given in Appendix B. The large number of events precludes a detailed presentation of each, and while each charging case is unique in some manner, many of the events are similar in location.

6.3.2 Location of Charging Events

The locations of the charging events listed in Appendix A are shown in Figure 13. Magnetic latitudes range from 64.8° N to 83.4° N, but 85 percent of the events are between 68° N and 75°N, and while magnetic local times range from 1738 to 0206, 82 percent of the events are between 2100 and 0100. The events are sorted by orbit and are depicted in Figures 14 (F6) and 15 (F7) which show that the lack of events identified in the post-midnight sector is not due to limited orbital coverage. All charging occurred either within full shadow of the earth or occasionally just along the eclipse border such that the SSJ/4 instrument remained in shadow. The dependence on magnetic location and darkness also yields a UT dependence as nearly 70 percent of the events occurred between 0630 and 1830 UT. The durations of these events range from one second to one minute and illustrate the variability of the charging currents, and the high energy precipitating electrons are a charging current source of particular interest.
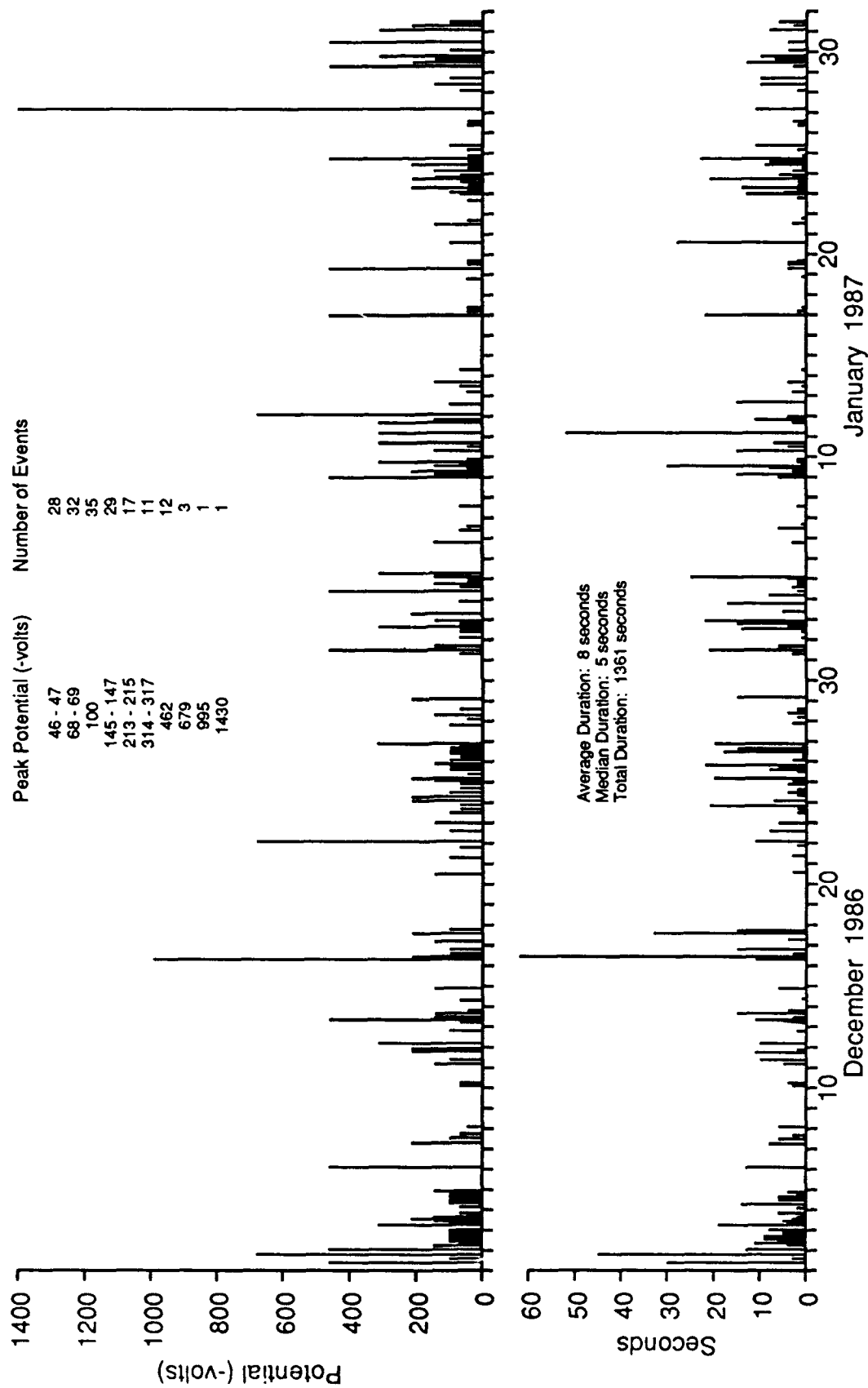
Fig. 12. DMSP charging levels and durations of events occurring during solar minimum.
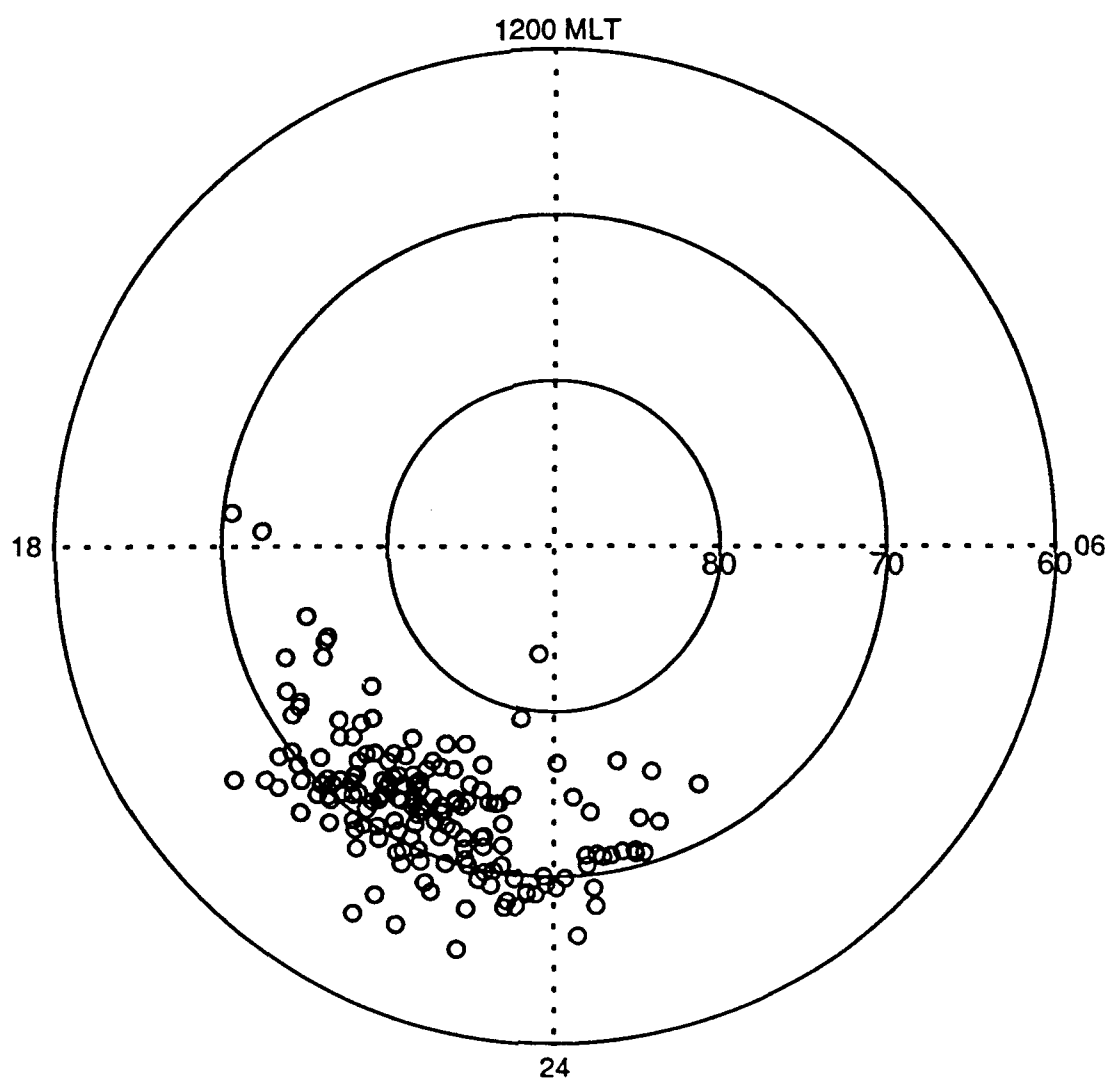
Fig. 13. Positions of F6 and F7 satellites in corrected geomagnetic latitude and magnetic local time during solar minimum charging events. Each circle represents the location of the greatest charging potential.
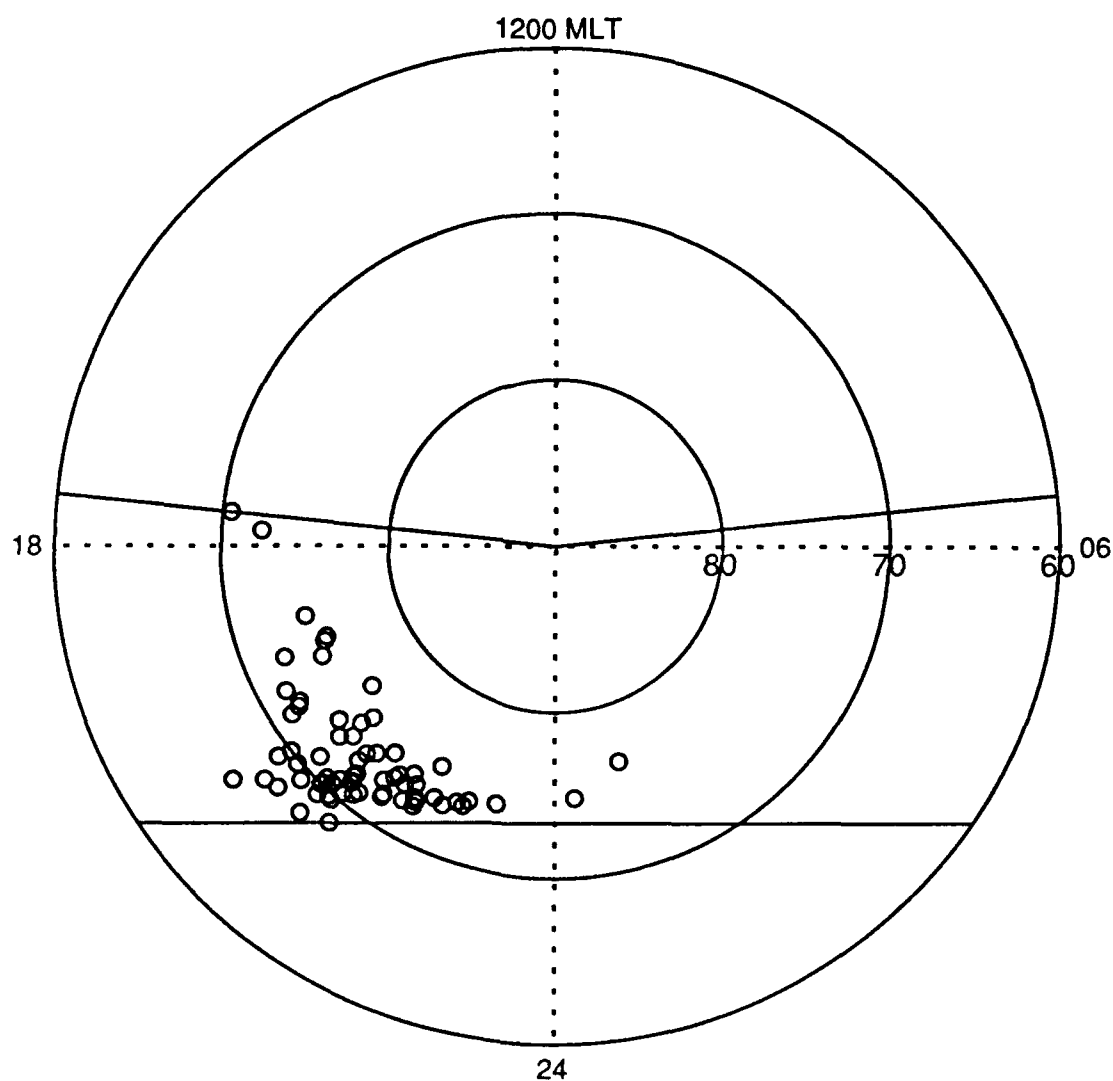
Fig. 14. Positions of F6 satellite in corrected geomagnetic latitude and magnetic local time during solar minimum charging events. Each circle represents the location of the greatest charging potential, and the solid lines define the orbital coverage.
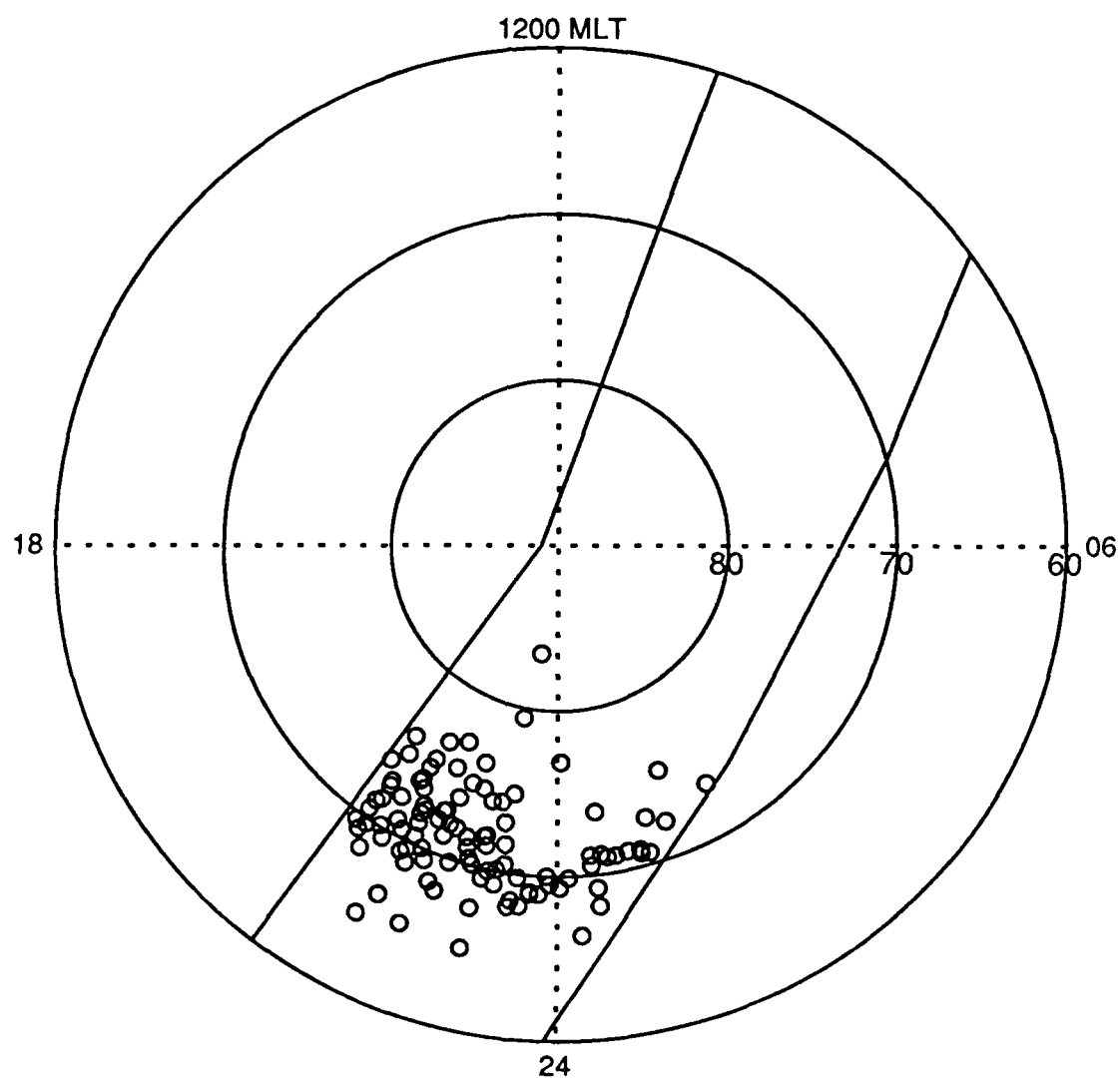
Fig. 15. Positions of F7 satellite in corrected geomagnetic latitude and magnetic local time during solar minimum charging events. Each circle represents the location of the greatest charging potential, and the solid lines define the orbital coverage.

6.3.3 Analysis of Electron Precipitation

Energetic electrons are accepted as a primary cause of significant negative spacecraft charging. To characterize the electron population during the charging events of solar minimum, Figures 16 and 17 depict plots of total electron flux and ≥9.6 keV electron flux, respectively, versus charging magnitude. As expected, the correlation of total electron flux to charging magnitude is weak, and these fluxes range over one order of magnitude for a given potential. The ≥9.6 keV plot depicts a better correlation of electron flux to potential, but the fluxes extend over a large range particularly at lower charging levels. The unorderedness and broad range of this latter plot are due to four factors; first, the ambient plasma densities probably vary for different events, and as *Gussenhoven, et al.* [1985] demonstrated, the ratio of high energy electron flux to ambient density provides a more ordered relationship; second, the electron population below 1000 eV may create more than one secondary electron for each incident electron and inhibit charging; third, electrons between 2-9 keV probably contribute toward charging; and finally, electron fluxes beyond the SSJ/4's energy range may be adding to the charge imbalance. While the better correlation includes the ≥9.6 keV electrons, events demonstrate that lesser energetic electrons can drive DMSP charging.

6.3.4 Contributions of Less Energetic Electrons

Though the study of *Gussenhoven et al.* [1985] showed a direct relationship between significant DMSP charging and enhanced fluxes of electrons with energies from 14-30 keV, electrons of lesser energy may also produce a significant charge imbalance. The -100 volt event on January 31, 1987, at 093207 UT is due in part to precipitating electrons with energies from 2-6.5 keV which make up over 90 percent of the electron population. Electrons of higher energy contribute only four hundredths of a percent toward total flux during this event (see Appendix B). Furthermore, electron populations during -45 to -69 volt charging events suggest that 2-4.5 keV electrons can
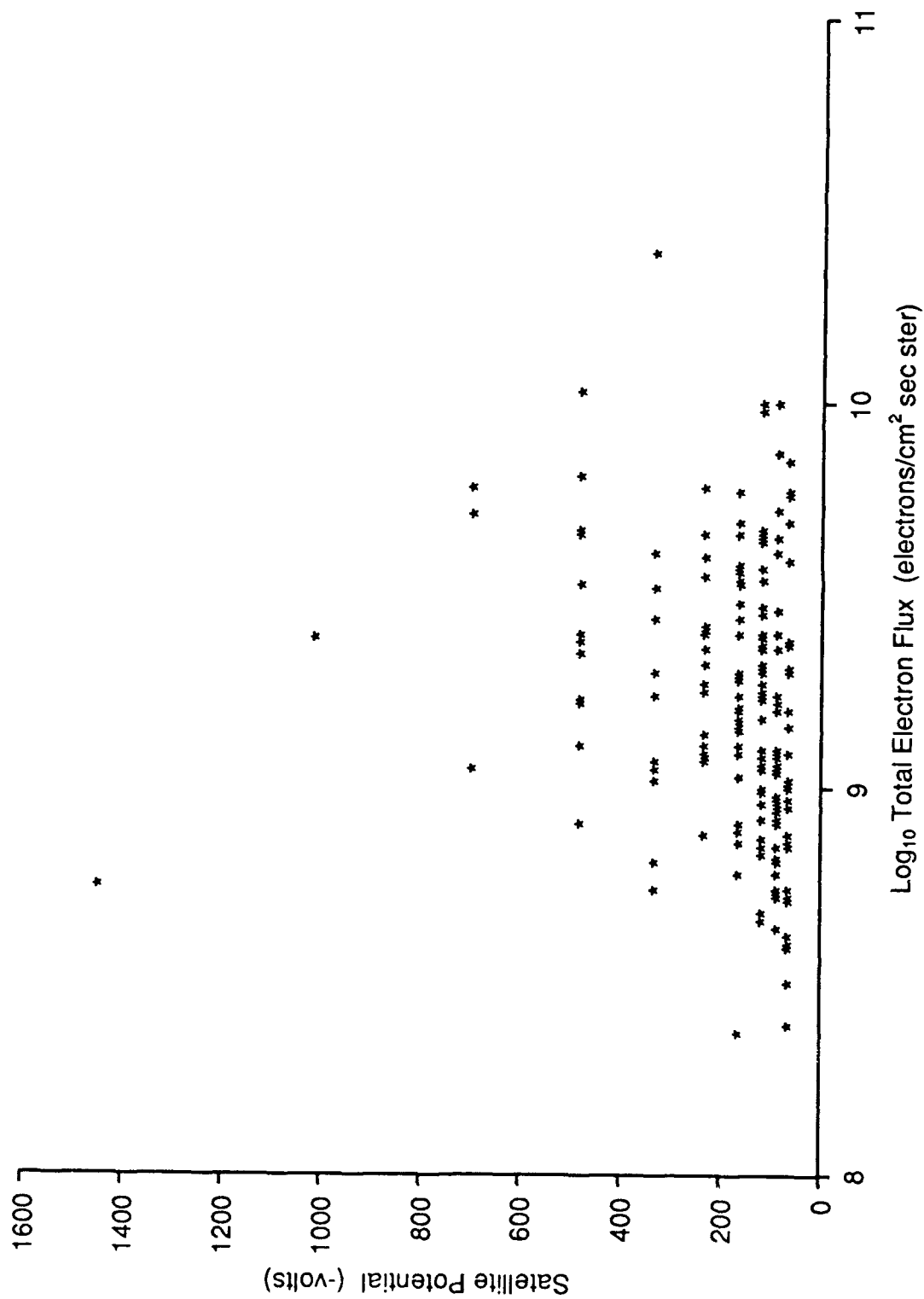
Fig. 16. Satellite potential plotted as a function of the total electron integral number flux.

58
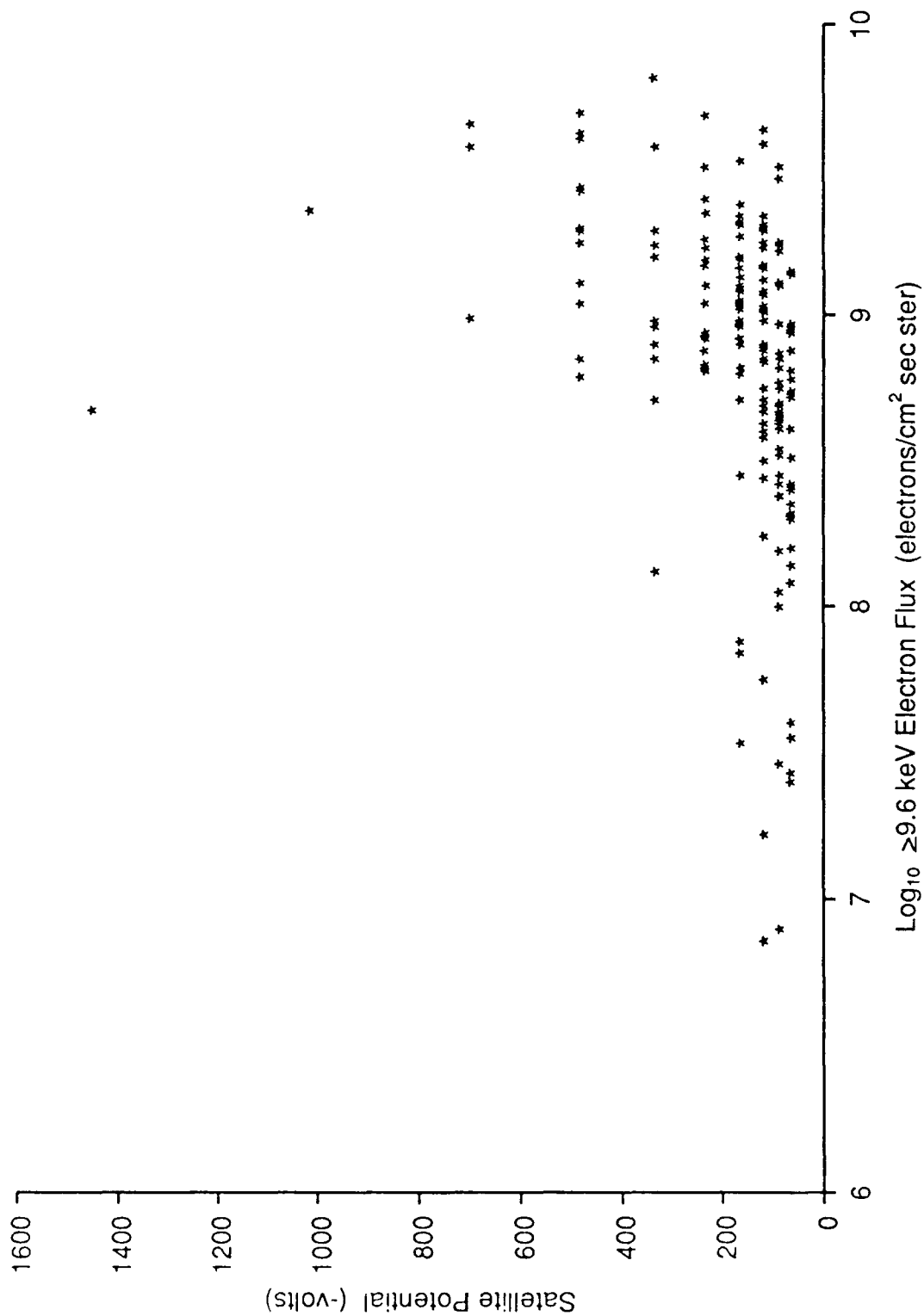
Fig. 17. Satellite potential plotted as a function of the electron integral number flux for energies ≥ 9.6 keV.

drive charging. Though other current sources such as ambient plasma may enhance the probability or severity of charging, no source other than these precipitating electrons appears capable of generating the charge imbalance necessary to achieve such negative potentials. Considering that 2-4.5 keV electrons likely contribute to charging and that incident electrons at lower energies limit charging, a further analysis of the electron populations during the charging events is necessary.

6.3.5 Effects of Secondary Electrons

The ratio of the ≥ 3.05 keV electron flux to the total electron flux during charging illustrates the effect of enhanced secondary electron production due to precipitating electrons ≤ 1 keV. Table 7 lists three groups of events based on charging level. Of particular interest is a comparison of group B to group C. The percent of events having large fluxes of ≥ 3 keV electrons is the same for groups B and C, but the electron populations for over 80 percent of the group C events are 90 percent energetic while only half of the group B events are 90 percent energetic. This illustrates that group C

TABLE 7. Electron Spectra Characteristics During Solar Minimum Charging Events

Group	A	B	C
Charging Level (-volts)	45-69	100-215	≥ 314
Number of Events	60	81	28
% of Events with ≥ 3 keV Fluxes $>10^{9.1}$ (electrons/ cm^2 sec ster)	32%	65%	64%
% of Events with ≥ 3 keV Flux/Total Flux $\geq 90\%$	38%	50%	82%

events have fewer incident electrons ≤1 keV, and therefore, fewer secondary electrons are generated. The lower DMSP charging levels of group A include not only decreased ≥3 keV fluxes, but also higher percentages of lower energy electrons. Two charging cases during solar minimum exemplify the process of large fluxes of energetic electrons combining with small fluxes of lower energy electrons (group C events) to generate severe negative potentials.

6.3.6 DMSP Severe Charging

The -1.43 kilovolt and -995 volt charging events on January 27, 1987, and December 16, 1986, respectively, represent the two largest DMSP negative potentials reported to date (see Appendix B). Both occurred near 70° N magnetic latitude and at 2215 magnetic local time. The precipitating electron spectra during both events are similar in that the greatest number flux is due to particles ≥20 keV, and both spectra suggest that significant electron fluxes exist beyond 30 keV. In particular, the -1.43 kilovolt event has relatively small electron fluxes below 20 keV and shows a logarithmically steady flux increase from 10 keV to 30 keV. A plot of the electron fluxes above 1 keV for both events is shown in Figure 18. Unfortunately, the detectors' ranges do not permit a more adequate description of the electron spectra driving these extreme potentials. Another feature of these two events and many others is the quickness in which the charging levels react to the onset, fluctuation, and end of energetic electron precipitation.

6.3.7 Time Constants

The charging and discharging of the DMSP satellites often appears instantaneous with the onset and end of energetic electron precipitation. That is, during the first second in which the SSJ/4 measures a significant increase or decrease in energetic electron flux, the SSJ/4 also measures an increase or decrease in potential during that second. However, the manner in which the SSJ/4 measures particles of various
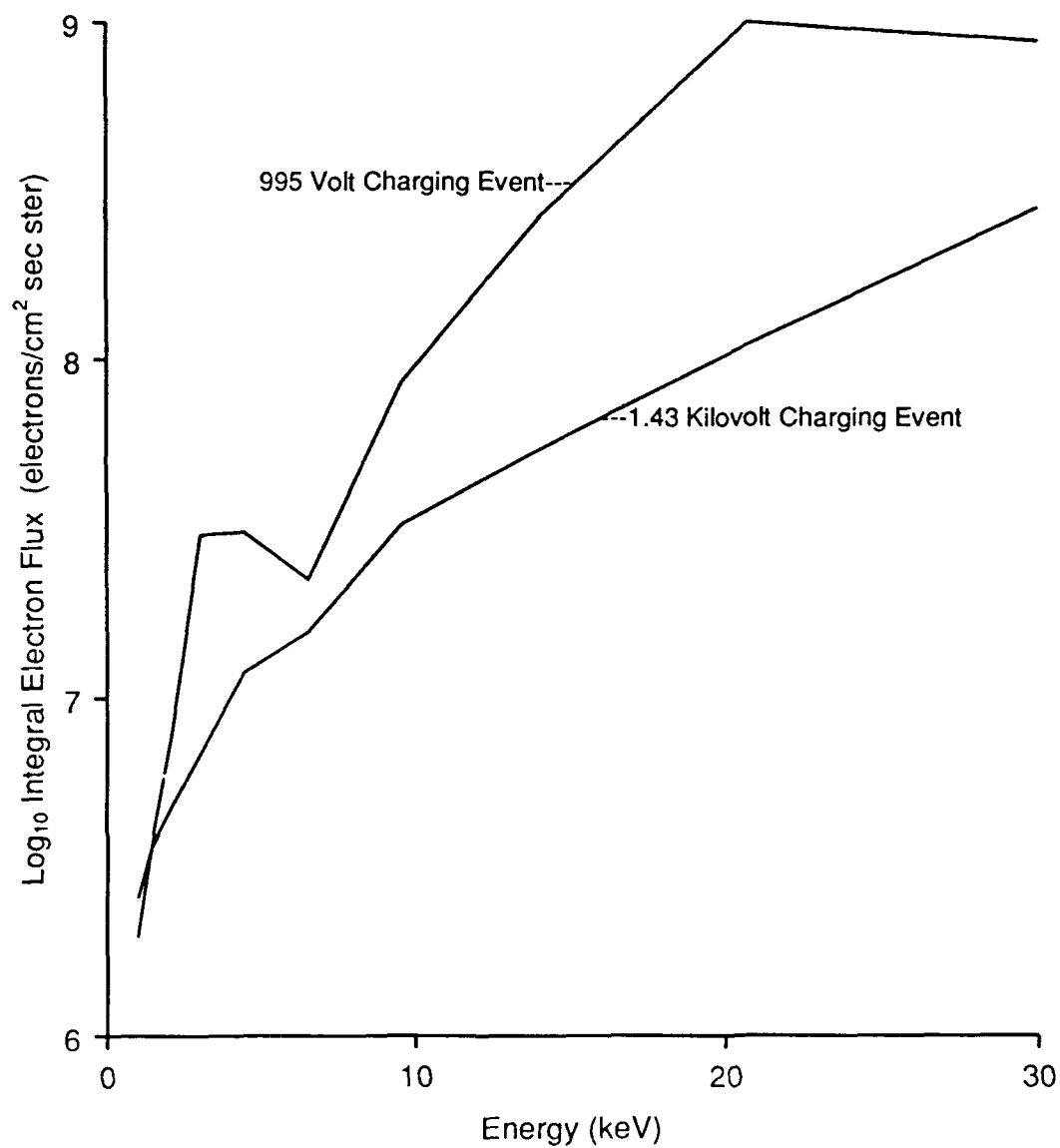
Fig. 18. Electron integral number fluxes for energies above 1 keV during two extreme DMSP charging events.

energies (changing channels every tenth of a second) limits an absolute characterization of the time constants. The satellites often appear to react as fast as .1 seconds (possibly faster), and rarely does this time constant exceed a full second. This seemingly short time constant is the rule rather than the exception for the events listed in Appendix A and shown in Appendix B and falls within the theoretical range of .002 seconds (conductor) to 1.6 seconds (dielectric) for a 1-kilovolt potential to form on a sphere with a radius of 1 meter [*Katz et al.*, 1977b] as noted in section 2.1. The few exceptions may be due to changing thermal plasma densities which affect the charging levels, and this important current source is now examined with the use of a model.

6.3.8 Model Ambient Plasma Densities

Though not a substitute for real measured data, the TDIM characterizes the plasma density for various conditions and locations. To illustrate the high-latitude plasma pattern predicted by the model, plasma densities at 800 kilometers and 1300 UT for solar minimum, winter, low Kp, and interplanetary magnetic field B_y positive conditions are shown in Figure 19. Arrows identify the regions of most interest for this study. Region A represents the polar hole, a region of significantly depleted plasma. Regions B and C denote pre- and post-midnight regions of aurorally enhanced plasma density. Further equatorward, region D depicts the mid-latitude trough. The general features shown in Figure 19 do not change significantly for varying conditions of Kp, UT, and so ar flux. However, the location of the polar hole for B_y negative conditions is centered near 0200 MLT rather than near 2200 MLT, so the plasma patterns can change often. The modeled densities within the key regions may be compared for various conditions. TDIM plasma densities for solar minimum, medium, and maximum, and low and medium Kp activities are shown in Table 8. Densities are lowest in all regions during solar minimum and range over one order of magnitude or more from solar minimum to solar maximum within the polar hole and mid-latitude

63
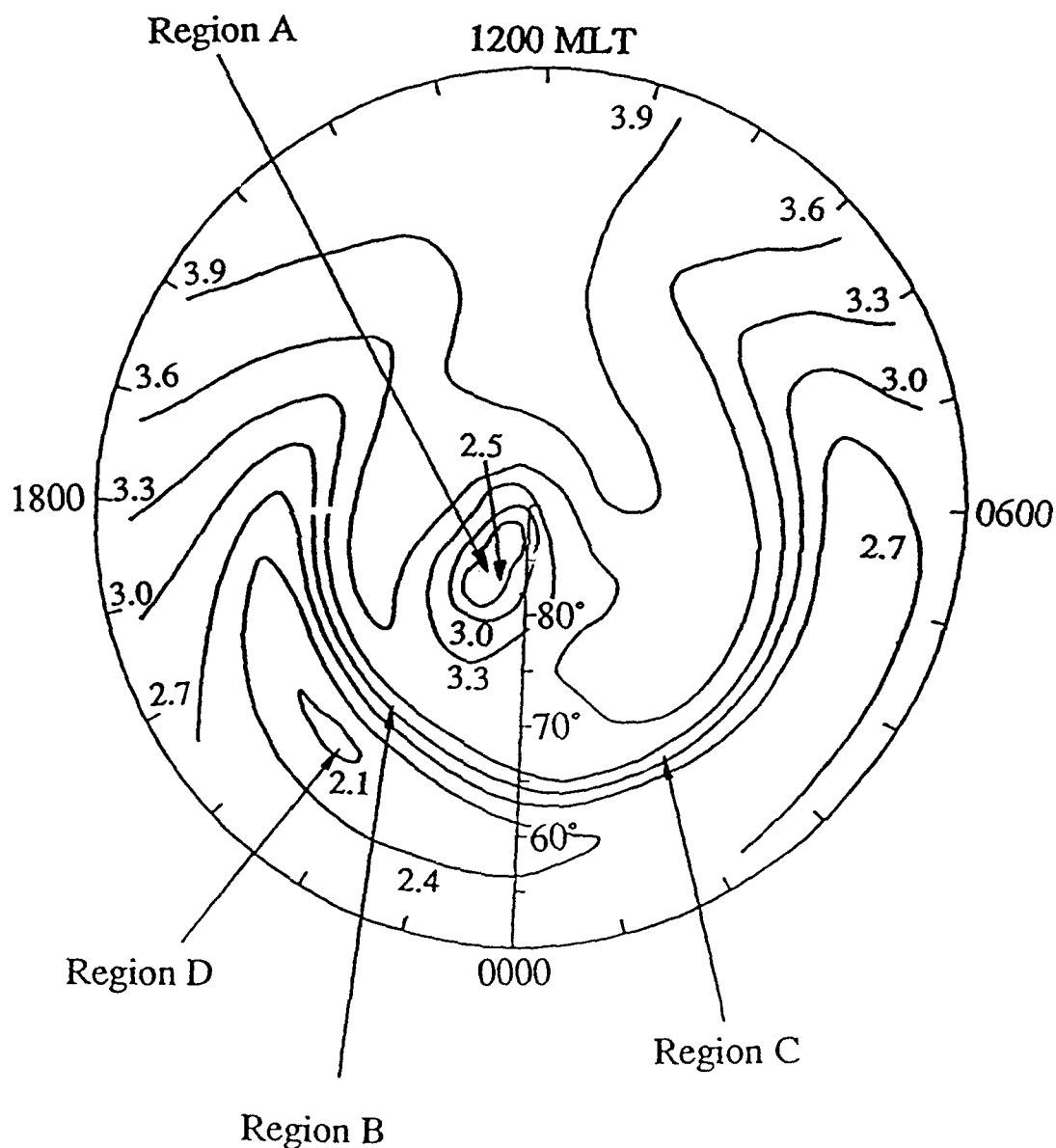
Fig. 19. TDIM-generated plasma pattern and densities ($\log_{10}$) at 800 kilometers during a winter period of low solar flux and low magnetic activity. The plot is in corrected geomagnetic latitude and magnetic local time and is valid for 1300 UT, and the contours represent constant plasma densities.

TABLE 8. Model Ambient Plasma Densities (Log_{10} cm^{-3}) at 800 Kilometers and 1300
UT for Three Levels of Solar Flux and Low and Medium Levels of Magnetic Activity

10.7 cm Solar Flux	70	130	210
K_p Level	1/3.5	1/3.5	1/3.5
Region A (polar hole)	2.48/2.80	2.90/3.40	3.40/3.80
Region B (aurorally enhanced 2200MLT)	3.72/3.95	4.05/4.30	4.35/4.55
Region C (aurorally enhanced 0200MLT)	3.70/3.70	3.90/4.10	4.25/4.25
Region D (mid-latitude trough)	1.91/2.25	2.54/3.00	3.21/3.50

trough. Densities in the aurorally enhanced regions during solar maximum are 3.5 to 4.5 times greater than during solar minimum, and in general, model densities for solar maximum are consistent with the SSIES data studied in Chapter V. While a significant variation over a solar cycle is predicted, the densities during solar minimum are of special interest.

Considering the location of most of the charging events, the area of primary interest includes the transition between the polar hole and pre-midnight aurorally enhanced region. Model densities in this area range from 3.0×10^2 cm^{-3} to 5.2×10^3 cm^{-3} and represent values consistent with those encountered during the DMSP charging events reported by *Gussenhoven et al.* [1985]. The location of the polar hole's equatorward boundary is due to a statistical model input of auroral precipitation at high magnetic latitudes which limits the southern extension of the hole. In the absence of auroral precipitation, the decreased plasma densities of the polar hole would then extend equatorward into the region of observed charging. The ambient plasma does not react

fully to the onset of auroral precipitation for nearly 30 minutes (J.J. Sojka, private communication, 1990), so a satellite could orbit through a region of depleted plasma and electron precipitation simultaneously. While the model suggests that plasma densities are considerably lower during solar minimum than solar maximum and that solar minimum densities are low enough for charging to occur based on the results of *Gussenhoven et al.* [1985], the possibility that charging occurred more often during solar minimum because of more energetic or frequent high energy electron precipitation must be considered.

6.3.9 Frequency of Energetic Electron Precipitation

The total number of seconds that the F6 and F7 satellites encountered intense energetic electron precipitation is shown in Table 9, and the total time that the satellites encountered intense electron precipitation of lesser energy is shown in Table 10; the percent of the total time that each was encountered is shown in parentheses. The values in brackets represent the percent this solar minimum value is of that measured during solar maximum for the same period. The amount of time the DMSP reported data during December and January was only slightly greater during solar minimum, so the percentages provide for a valid comparison. While enhanced total electron precipitation was encountered more often during solar minimum, the fluxes of high energy electrons shown to generate charging were virtually the same during these periods. During solar minimum and in great contrast to solar maximum, periods for which ≥ 9.6 keV electron fluxes exceeded 3.0×10^8 electrons/(cm^2 sec ster) in darkness for more than two seconds resulted in negative charging (>45 volts) more than 50 percent of the time. The apparent dependence of charging on energetic electron precipitation warrants a consideration of a Kp to charging relationship.

6.4.0 Kp to Charging Relationship

Though at least one study of geosynchronous orbit charging has reported a

TABLE 9. Frequency (seconds) of $\geq 9.6 \text{keV}$ Electron Fluxes Greater than $10^{8.5}$ (electrons/cm^2 sec ster) During Solar Minimum

Satellite	F6	F7
December 1986	773 (.14%) [146%]	502 (.09%) [71%]
January 1987	370 (.06%) [89%]	528 (.09%) [99%]
Total: 2171 [99.5%]		

Values in parentheses represent the percentage of the total time that the satellites encountered these fluxes poleward of 50° N magnetic latitude.

Values in brackets represent the percentage that this solar minimum frequency is of the solar maximum frequency for similar orbits and months.

TABLE 10. Frequency (seconds) of Total Electron Fluxes Greater than $10^{9.3}$ (electrons/cm^2 sec ster) During Solar Minimum

Satellite	F6	F7
December 1986	3039 (.55%) [174%]	4017 (.72%) [125%]
January 1987	2185 (.37%) [147%]	3855 (.66%) [140%]
Total: 13,096 [142%]		

Values in parentheses represent the percentage of the total time that the satellites encountered these fluxes poleward of 50° N magnetic latitude.

Values in brackets represent the percentage that this solar minimum frequency is of the solar maximum frequency for similar orbits and months.

positive correlation between Kp level and charging [*Mullen et al.,* 1986], little correlation exists between the Kp index and the occurrence or severity of DMSP charging. The relationship between the 3 hour Kp indexes and satellite potentials is shown in Figure 20. The Kp values extend through a broad range for a given potential, and the larger Kp values do not correspond to greater potentials. Moreover, charging occurs throughout the Kp range of solar minimum. The nature of the Kp index (3 hour, global scale) coupled with the other current sources which control LEO charging limits the use of Kp as an indicator of high-latitude spacecraft charging. An auroral electrojet (AE) index may be better suited to identify localized currents of short duration, but the AE index is not readily available like the Kp. Both the Kp and AE indexes may show a better correlation if the ambient plasma densities during the charging events were known and considered.

The analysis of the solar minimum data base is complete. The numerous charging events during solar minimum and the lack of charging events during solar maximum represent a significant solar cycle dependence. A discussion of the results from these two periods is now presented.
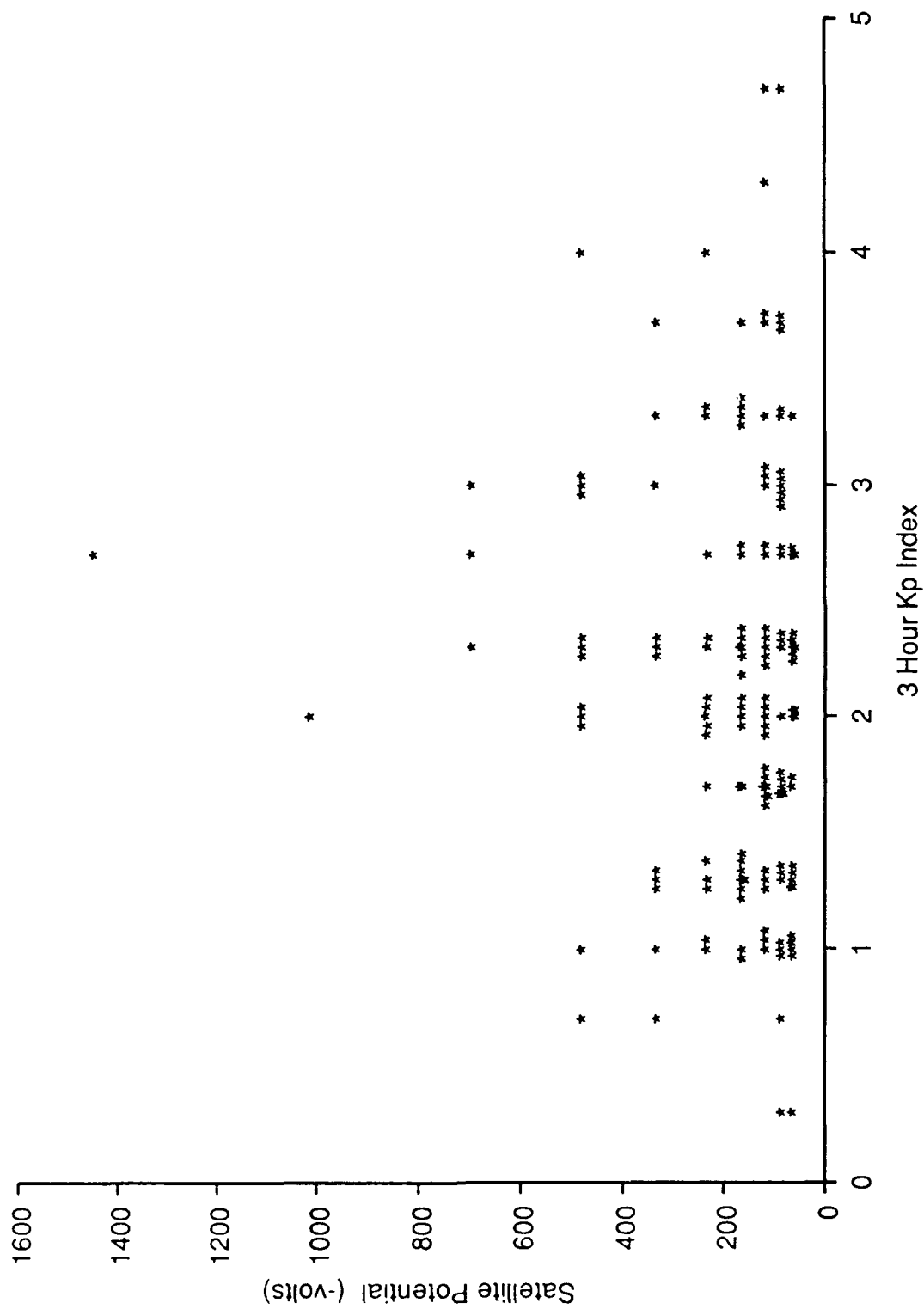
Fig. 20. Satellite potential plotted as a function of the 3 hour Kp index.

CHAPTER VII

DISCUSSION

7.1 Solar Cycle Dependence

One hundred seventy DMSP charging events were identified by an extensive search of F6, F7, F8, and F9 measurements taken during the winter months of 1986-87, and 1989-90. One hundred sixty nine of the events, including the most severe DMSP potential ever reported (-1.4 kilovolts), occurred during solar minimum conditions while only one event occurred during solar maximum conditions. The primary current sources which can generate or inhibit these DMSP charging levels are photoemission, precipitating ions, precipitating electrons and their secondary electrons, and ambient ions. Thus, a significant variation during the solar cycle of one or more of these current sources is believed to be responsible for the distinct difference in results.

7.1.1 Photoemission

Since nearly all charging events occurred in full shadow of the earth, and the amount of time the satellites spent in eclipse during the two periods was virtually the same, a varying photoemission rate could not have caused the disparity in results. However, the significance of photoemission is not diminished as the absence of significant charging in sunlight suggests that solar radiation strongly inhibited DMSP charging. Also, a photoionization-caused increase of ambient ion density across the eclipse may have also contributed to a lack of sunlight charging.

7.1.2 Precipitating Ions

Enhanced ion precipitation occasionally contributed toward current balance by occurring simultaneously with energetic electron precipitation, but the frequency of this

phenomenon was insignificant. Furthermore, simultaneous electron/ion precipitation did not occur more often during solar maximum than solar minimum, so a variation of ion precipitation did not contribute to the charging solar cycle dependence.

7.1.3 Precipitating Electrons and Ambient Ions

The frequency and distribution of energetic electron precipitation did not vary significantly between the periods of study, and electron precipitation which generated charging during solar minimum did not cause charging during solar maximum. In contrast to the lack of variability in energetic electron precipitation over the solar cycle, the TDIM predicts at least an order of magnitude ambient plasma density variation between solar maximum and minimum, and the model data compares closely to the measured data of solar maximum as well as the experimental data of *Gussenhoven et al.* [1985]. The ambient plasma density during the single solar maximum charging event was one of the lowest during the period. Though the solar minimum analysis lacks measured thermal plasma data, ambient plasma appears to be the chief current source which varied over the solar cycle. Therefore, the solar cycle control of ambient plasma density is responsible for the spacecraft charging to solar cycle relationship.

7.2 Electrons Generating a Potential

Many studies emphasize that a flux of "energetic" electrons is necessary in order to generate significant negative potentials. Though DMSP charging levels during solar minimum correlated better to fluxes of high energy electrons (≥ 9.6 keV) than to total electron fluxes, potentials as large as -100 volts occurred during periods of ≤ 6.5 keV electron precipitation (assuming no fluxes beyond the energy range of the detector occurred simultaneously). Theoretical secondary electron yields for kapton, the primary material of DMSP satellites, predict less than one secondary electron per incident electron above 1-? keV. Coupled with the theoretical expectation that nearly one tenth of

the incident electrons will backscatter, the suggestion that charging may be due to electrons as low as 2 keV seems reasonable if fluxes at lower energies are relatively small. Of course, the number flux necessary at these energy levels to create a significant charge imbalance is so large that charging is less frequent and severe without higher energy electron fluxes. Moreover, intense electron fluxes above 2 keV can generate significant DMSP charging levels.

The concept of material-dependent critical electron temperatures (E_T) and energies (E_E) being necessary to generate a surface charge imbalance is described in *Laframboise and Kamitsuma* [1983], *Lai et al.* [1983], and *Katz et al.* [1986]. The temperature of a Maxwellian distribution must exceed E_T for the incident electrons to outnumber the secondary and backscattered electrons, and at the same time, electrons with energies greater than E_E are necessary regardless of temperature for charging to occur. The values of E_T and E_E for kapton range from .5 to .8 keV and 1.2 to 4.0 keV, respectively, depending on the angle of electron incidence and the backscatter and secondary coefficients used [*Lai et al.*, 1983; *Katz et al.*, 1986]. This concept was not specifically addressed in this study because of the Maxwellian dependence, but the theoretical E_E range is consistent with the observed energy range discussed in the previous paragraph.

7.3 The Role of Secondary Electrons

Precipitating electrons below a material-dependent energy level inhibit negative charging by creating multiple secondary electrons. On two occasions during solar maximum, the ambient plasma density was lower and the high energy electron fluxes were greater than during the solar maximum charging event. However, the electron fluxes below 1 keV were also greater and probably inhibited a potential from forming. Furthermore, a large percentage of the most severe charging events during solar minimum occurred when over 90 percent of the electron flux was at or above 3 keV, and

many of the least severe charging events during solar minimum had equally large fluxes at higher energies, but also had greater fluxes of low energy electrons. These results further suggest that 1-2 keV is a key electron energy for DMSP charging.

7.4 Ambient Plasma Densities

From model outputs and experimental results, an ambient plasma density of 10^4 cm^{-3} may be considered as a rough threshold for DMSP charging assuming precipitating electron distributions are similar to those of this study and of *Gussenhoven et al.* [1985]. The TDIM predicts densities below 10^4 cm^{-3} during solar minimum and above 10^4 cm^{-3} during solar maximum for much of the nightside at 800 kilometers. The measured plasma density during the weak charging event of solar maximum was just above 10^4 cm^{-3} while the densities for 10 out of the 11 charging events reported by *Gussenhoven et al.* [1985] were below 10^4 cm^{-3}. The electron fluxes causing charging during solar minimum did not cause charging during solar maximum when the measured ambient plasma densities were above 10^4 cm^{-3}.

7.5 Location of Events

Most of the charging events during solar minimum occurred between 68°N-75°N magnetic latitude and 2100-0100 magnetic local time. Events in the post-midnight sector were less frequent even though satellite coverage in this region was significant. As already discussed, the TDIM predicts the position of the polar hole to vary between the pre- and post-midnight sectors depending on the interplanetary magnetic field's B_y component. Hence, regions of lower ambient plasma density excluding the effects of electron precipitation are not expected to show significant tendencies toward one region or the other. In contrast, electron precipitation is often discrete and more energetic in the pre-midnight sector and diffuse in the morning sector. Considering the electron populations which generate charging, it appears that while the ambient plasma densities

largely control whether charging will occur, the energetic electron precipitation controls where the charging will occur.

7.6 Charging at Lower Altitudes

With polar orbit charging at 800 kilometers largely a function of ambient plasma density and energetic electron precipitation, the frequency and severity of charging are likely to decrease as altitude decreases. The TDIM predicts densities as low as 5.6×10^3 cm^{-3} at 300 kilometers within the polar hole for solar minimum conditions. If 10^4 cm^{-3} is indeed an accurate threshold, significant charging is possible even as low as 300 kilometers and would be limited by the fluxes of energetic electrons. The energy degradation between 800 and 300 kilometers of precipitating particles is non-trivial, but not to the extent of significantly softening electrons in the 1-30 keV energy range. Thus, significant spacecraft charging appears to be possible during solar minimum even near the high-latitude nightside F2 layer peak. While further study is necessary to form conclusions concerning spacecraft charging in this lower region, the extensive data base, analyses, and results of this study lead to conclusions which enhance the understanding of spacecraft charging within the high-latitude upper ionosphere.

CHAPTER VIII

CONCLUSION

The primary causes, frequency, severity, and solar cycle dependence of high-latitude spacecraft charging in low-earth polar orbit (840 kilometers) have been identified from extensive satellite measurements during northern hemispheric winter periods of solar maximum and minimum. The environments generating satellite-to-plasma potential differences were analyzed using measured precipitating particle and ambient plasma data as well as model ambient plasma data, and the environments which did not cause spacecraft charging were similarly examined.

8.1 Conclusions

As a result of these analyses, the following conclusions represent new experimental findings in the study of LEO spacecraft charging: (1) An extreme solar cycle dependence exists; the solar minimum environment generates charging more frequently and with greater magnitude. (2) The chief cause of this dependence is a solar cycle variation of ambient plasma density; the lack of significant charging during solar maximum is due to high ambient plasma densities. (3) Kilovolt charging can occur via natural processes within low-earth orbit. (4) Electrons with energies from 2-5 keV contribute to charging though higher energy electrons make greater contributions. Integral number fluxes for electrons ≥ 9.6 keV are on the order of 10^8-10^{10} electrons/(cm^2 sec ster) when negative potentials >100 volts form. (5) Incident electrons with energies below 1 keV inhibit charging by producing multiple secondary electrons. (6) The Kp index is not a strong indicator of charging. The final two conclusions are consistent with those of *Gussenhoven et al.* [1985]: (7) A thermal plasma density of 10^4 cm^{-3} or less is required for significant charging to occur. (8)

Charging is most common in the pre-midnight magnetic frame within the earth's shadow near 70°N latitude.

8.2 Recommendations for Further Study

Progress toward further understanding of high-latitude ionospheric charging may be achieved through additional research. Recommended methods include examining charging environments during various solar flux conditions and/or during different seasons. Also, the electron spectra and ambient plasma resulting in different charging levels could be analyzed more closely to fine tune critical energy and density values and to better understand the physical processes which generate electric potentials. An attempt to experimentally quantify all currents, particularly those due to secondary emission, may benefit modeling efforts. Finally, a study of low-earth orbit charging within the southern hemisphere where the TDIM predicts deeper and broader polar density depletions may yield more severe charging.

REFERENCES

Balmain, K.G., Arc propagation, emission, and damage on spacecraft dielectrics, in *The Aerospace Environment at High Altitudes and its Implications for Spacecraft Charging and Communications, AGARD-CP-406*, p. 16-1, North Atlantic Treaty Organization, France, 1987.

Besse, A.L., and A.G. Rubin, A simple analysis of spacecraft charging involving blocked photoelectron currents, *J. Geophys. Res., 85*, 2324, 1980.

Broihanne, L., Spacecraft protection against electrostatic discharge--Application to the ARABSAT spacecraft, in *The Aerospace Environment at High Altitudes and its Implications for Spacecraft Charging and Communications, AGARD-CP-406*, p. 22-1, North Atlantic Treaty Organization, France, 1987.

DeForest, S.E., Spacecraft charging at synchronous orbit, *J. Geophys. Res., 77*, 651, 1972.

Frank, L.A., and K.L. Ackerson, Local time survey of plasma at low altitude over the auroral zone, *J. Geophys. Res., 76*, 3612, 1971.

Garrett, H.B., The charging of spacecraft surfaces, *Rev. Geophys., 19*, 577, 1981.

Garrett, H.B., and S.E. DeForest, Time varying photoelectron flux effects on spacecraft potential at geosynchronous orbit, *J. Geophys. Res., 84*, 2083, 1979.

Grard, R., K. Knott, and A. Pedersen, Interactions between a large body and its environment in a low polar orbit, in *Proceedings of the Air Force Geophysics Laboratory Workshop on Natural Charging of Large Space Structures in Near Earth Polar Orbit*, edited by R.C. Sagalyn, D.E. Donatelli, and I. Michael, *Rep. AFGL-TR-83-0046, ADA134894*, p. 175, Air Force Geophys. Lab., Hanscom Air Force Base, Mass., 1983a.

Grard, R., K. Knott, and A. Pedersen, Spacecraft charging effects, *Space Sci. Rev., 34*, 289, 1983b.

Greenspan, M.E., P.B. Anderson, and J.M. Pelagatti, Characteristics of the thermal plasma monitor (SSIES) for the Defense Meteorological Satellite Program (DMSP) spacecraft S8 through S10, *Rep. AFGL-TR-86-0227*, Air Force Geophys. Lab., Hanscom Air Force Base, Mass., 1986.

Gussenhoven, M.S., and E.G. Mullen, Geosynchronous environment for severe spacecraft charging, *J. Spacecraft Rockets, 20*, 26, 1983.

Gussenhoven, M.S., D.A. Hardy, F. Rich, W.J. Burke, and H.-C. Yeh, High-level spacecraft charging in the low-altitude polar auroral environment, *J. Geophys. Res., 90*, 11,009, 1985.

Hall, W.N., P. Leung, I. Katz, G.A. Jongeward, J.R. Lilley, Jr., J.E. Nanevicz, J.S. Thayer, and N.J. Stevens, Polar-auroral charging of the Space Shuttle and EVA astronaut, in *The Aerospace Environment at High Altitudes and its Implications for Spacecraft Charging and Communications, AGARD-CP-406,* p. 34-1, North Atlantic Treaty Organization, France, 1987.

Hardy, D.A., M.S. Gussenhoven, and D. Brautigam, A statistical model of auroral ion precipitation, *J. Geophys. Res., 94,* 370, 1989.

Hardy, D.A., M.S. Gussenhoven, and E. Holeman, A statistical model of auroral electron precipitation, *J. Geophys. Res., 90,* 4229, 1985.

Hardy, D.A., L.K. Schmitt, M.S. Gussenhoven, F.J. Marshall, H.-C. Yeh, T.L. Schumaker, A. Huber, and J. Pantazis, Precipitating electron and ion dectors (SSJ/4) for the block 5D/flights 6-10 DMSP satellites: Calibration and data presentation, *Rep. AFGL-TR-84-0317,* Air Force Geophys. Lab., Hanscom Air Force Base, Mass., 1984.

Katz, I., and M.J. Mandell, Differential charging of high-voltage spacecraft: The equilibrium potential of insulated surfaces, *J. Geophys. Res., 87,* 4533, 1982.

Katz, I., M. Mandell, G. Jongeward, and M.S. Gussenhoven, The importance of accurate secondary electron yields in modeling spacecraft charging, *J. Geophys. Res., 91,* 13,739, 1986.

Katz, I., D.E. Parks, M.J. Mandell, J.M. Harvey, D.H. Brownell, S.S. Wang, and M. Rotenberg, A three dimensional dynamic study of electrostatic charging in materials, *NASA Contract. Rep. CR-135256,* 1977a.

Katz, I., D.E. Parks, S. Wang, and A. Wilson, Dynamic modeling of spacecraft in a collisionless plasma, in *Proceedings of the Spacecraft Charging Technology Conference,* edited by C.P. Pike, and R.R. Lovell, *Rep. AFGL-TR-77-0051, ADA045459,* p.319, Air Force Geophys. Lab., Hanscom Air Force Base, Mass., 1977b.

Laframboise, J.G., Is there a good way to model spacecraft charging in the presence of space-charge coupling, flow, and magnetic fields?, in *Proceedings of the Air Force Geophysics Laboratory Workshop on Natural Charging of Large Space Structures in Near Earth Polar Orbit,* edited by R.C. Sagalyn, D.E. Donatelli, and I. Michael, *Rep. AFGL-TR-83-0046, ADA134894,* p. 57, Air Force Geophys. Lab., Hanscom Air Force Base, Mass., 1983.

Laframboise, J.G., and M. Kamitsuma, The threshold temperature effect in high-voltage spacecraft charging, in *Proceedings of the Air Force Geophysics Laboratory Workshop on Natural Charging of Large Space Structures in Near Earth Polar Orbit,* edited by R.C. Sagalyn, D.E. Donatelli, and I. Michael, *Rep. AFGL-TR-83-0046, ADA134894,* p. 293, Air Force Geophys. Lab., Hanscom Air Force Base, Mass., 1983.

Laframboise, J.G., and L.W. Parker, Spacecraft charging in the auroral plasma: Progress toward understanding the physical effects involved, in *The Aerospace Environment at High Altitudes and its Implications for Spacecraft Charging and Communications*, AGARD-CP-406, p. 13-1, North Atlantic Treaty Organization, France, 1987.

Lai, S.T., M.S. Gussenhoven, and H.A. Cohen, The concepts of critical temperature and energy cutoff of ambient electrons in high voltage charging of spacecraft, *Eur. Space Agency Spec. Publ., ESA SP-198*, 169, 1983.

Langmuir, I., and K. Blodgett, Currents limited by space charge between concentric spheres, *Phys. Rev., 24*, 49, 1924.

Leung, M.S., M.B. Tueling, and E.R. Schnauss, Effects of secondary electron emission on charging, Spacecraft charging technology 1980, *NASA Conf. Publ. 2182/AFGL-TR-81-0270*, p. 163, NASA, Greenbelt, Md.,1981.

Lin, C.S., and R.A. Hoffman, Characteristics of the inverted-V event, *J. Geophys. Res., 84*, 1514, 1979.

Mullen, E.G., and M.S. Gussenhoven, High-level spacecraft charging environments near geosynchronous orbit, *Rep. AFGL-TR-82-0063*, Air Force Geophys. Lab., Hanscom Air Force Base, Mass., 1982.

Mullen, E.G., M.S. Gussenhoven, D.A. Hardy, T.A. Aggson, B.G. Ledley, and E. Whipple, SCATHA survey of high-level spacecraft charging in sunlight, *J. Geophys. Res., 91*, 1474, 1986.

Olsen, R.C., A threshold effect for spacecraft charging, *J. Geophys. Res., 88*, 493, 1983.

Olsen, R.C., Record charging events from Applied Technology Satellite 6, *J. Spacecraft Rockets, 24*, 362, 1987.

Olsen, R.C., C.E. McIlwain, and E.C. Whipple, Jr., Observations of differential charging effects on ATS 6, *J. Geophys. Res., 86*, 6809, 1981.

Parker, L.W., Differential charging and sheath asymmetry of nonconducting spacecraft due to plasma flows, *J. Geophys. Res., 83*, 4873, 1978.

Parks, D.E., and I. Katz, Charging of a large object in low polar earth orbit, Spacecraft charging technology 1980, *NASA Conf. Publ. 2182/AFGL-TR-81-0270*, p. 979, NASA, Greenbelt, Md., 1981.

Prokopenko, S.M.L., and J.G. Laframboise, High-voltage differential charging of geostationary spacecraft, *J. Geophys. Res., 85*, 4125, 1980.

Raitt, W.J., Space Shuttle charging results, in *Proceedings of the Air Force Geophysics Laboratory Workshop on Natural Charging of Large Space Structures in Near Earth Polar Orbit*, edited by R.C. Sagalyn, D.E. Donatelli, and I. Michael, *Rep. AFGL-TR-83-0046, ADA134894*, p. 107, Air Force Geophys. Lab., Hanscom Air Force Base, Mass., 1983.

Raitt, W.J., J.V. Eccles, N.B. Myers, D.C. Thompson, P.M. Banks, P.R. Williamson, R.I. Bush, J. Hawkins, S. Sasaski, K.-I. Oyama, N. Kawashima, and W.F. Sharp, Active vehicle charging measurements in sounding rocket and Space Shuttle orbiter environments at low earth orbit (LEO) altitude, in *The Aerospace Environment at High Altitudes and its Implications for Spacecraft Charging and Communications, AGARD-CP-406*, p. 9-1, North Atlantic Treaty Organization, France, 1987.

Rosen, A., Spacecraft charging: Environment-induced anomalies, *J. Spacecraft Rockets, 13*, 129, 1976.

Schumaker, T.L., D.A. Hardy, S. Moran, A. Huber, J. McGarity, and J. Pantazis, Precipitating ion and electron detectors (SSJ/4) for the block 5D/flight 8 DMSP satellite, *Rep. AFGL-TR-88-0030*, Air Force Geophys. Lab., Hanscom Air Force Base, Mass., 1988.

Schunk, R.W., A mathematical model of the middle and high latitude ionosphere, *Pure Appl. Geophys., 127*, 255, 1988.

Shaw, R.R., J.E. Nanevicz, and R.C. Adamo, Observations of electrical discharges caused by differential satellite charging, in *Spacecraft Charging by Magnetospheric Plasmas, Prog. Astronaut. Aeronaut., vol. 47*, edited by A. Rosen, p. 61, AIAA Press, New York, 1976.

Sojka, J.J., Global scale, physical models of the F region ionosphere, *Rev. Geophys., 27*, 371, 1989.

Whipple, E.C., Jr., Observation of photoelectrons and secondary electrons reflected from a potential barrier in the vicinity of ATS 6, *J. Geophys. Res., 81*, 715, 1976.

Whipple, E.C., Jr., An overview of charging of large space structures in polar orbit, in *Proceedings of the Air Force Geophysics Laboratory Workshop on Natural Charging of Large Space Structures in Near Earth Polar Orbit*, edited by R.C. Sagalyn, D.E. Donatelli, and I. Michael, *Rep. AFGL-TR-83-0046, ADA134894*, p. 11, Air Force Geophys. Lab., Hanscom Air Force Base, Mass., 1983.

Whipple, E.C., Jr., and R.C. Olsen, High spacecraft potentials on ISEE-1 in sunlight, in *The Aerospace Environment at High Altitudes and its Implications for Spacecraft Charging and Communications, AGARD-CP-406*, p. 8-1, North Atlantic Treaty Organization, France, 1987.

Yeh, H.-C, and M.S. Gussenhoven, The statistical electron environment for Defense Meteorological Satellite Program eclipse charging, *J. Geophys. Res., 92*, 7705, 1987.

APPENDICES

Appendix A: Summary of Charging Events

The charging events of solar minimum are listed in Table 11. The universal times (UT) are in hours, minutes, and seconds and represent the moment of greatest charging. The charging magnitudes (Φ) identify the highest potential level achieved during the event and are defined as the central energy of the SSJ/4 channel measuring the enhanced ion flux. MLAT and MLT are corrected geomagnetic latitude and magnetic local time, respectively, which mark the satellites' position at UT. The total duration of negative charging ≥ 46 volts during an event is shown by ΔT. The ion fluxes are the integral number fluxes (ions/cm^2 sec ster) in the charging channel; because of changing potential levels and the instruments' channel pass bands, the ion fluxes vary from event to event and do not reflect the severity of charging. The electron fluxes are integral number fluxes (electrons/cm^2 sec ster) at UT. An asterisk indicates significant electron fluxes beyond the detectors' range.

TABLE 11. Summary of Solar Minimum Charging Events

Day	UT	Satellite	Φ (-volts)	MLAT	MLT	ΔT (sec)	Log_{10} Ion Flux	Log_{10} Electron Fluxes	
								Total	$\geq 9.6\text{keV}$
12/1/86	093745	F6	462	72.1	2004	30	7.62	9.53	9.43
12/1/86	150606	F7	100	68.7	2349	3	6.60	9.18	9.03
12/1/86	180607	F6	679	68.6	2123	45	8.02	9.05	8.99
12/2/86	011718	F7	462	71.2	0024	13	7.39	9.66	9.61*
12/2/86	080408	F7	147	64.8	2205	4	7.02	9.57	9.34
12/2/86	091636	F6	68	71.7	1954	11	6.88	8.71	8.38
12/2/86	112320	F7	100	69.8	2245	6	7.60	9.24	9.08
12/2/86	124022	F6	100	67.7	2036	9	7.37	8.83	8.69
12/2/86	144537	F7	100	68.9	2343	9	7.12	9.62	9.17
12/2/86	160112	F6	100	72.2	2204	5	7.61	9.53	9.34
12/3/86	003250	F6	100	75.1	1933	8	6.62	9.27	9.01
12/3/86	060247	F7	314	69.3	2214	19	6.85	9.02	8.90
12/3/86	103534	F6	100	73.4	2036	4	6.56	8.94	8.67
12/3/86	110228	F7	147	72.0	2239	5	7.23	9.40	9.20
12/3/86	124345	F7	215	69.9	2311	3	8.10	9.55	9.40
12/3/86	124519	F7	147	65.0	2305	2	7.16	9.14	8.97
12/3/86	140014	F6	46	68.0	2045	1	6.91	8.60	8.51
12/3/86	153942	F6	68	72.5	2204	6	6.56	8.94	8.87
12/4/86	040021	F7	69	74.1	2304	2	6.70	8.94	8.69
12/4/86	072208	F7	100	70.9	2202	14	6.42	9.04	8.60
12/4/86	122250	F7	100	72.0	2307	6	6.71	9.47	9.07
12/4/86	133643	F6	100	72.6	2138	6	7.99	9.31	9.12

TABLE 11. Continued

Day	UT	Satellite	Φ (-volts)	MLAT	MLT	ΔT (sec)	Log_{10} Ion Flux	Log_{10} Electron Fluxes Total	$\geq 9.6 keV$
12/4/86	190816	F7	100	71.0	0100	2	7.60	9.99	8.63
12/4/86	223054	F7	147	73.2	0206	4	7.99	9.77	9.04
12/6/86	031935	F7	462	73.0	2318	13	7.96	9.37	9.25
12/7/86	062115	F7	215	72.4	2211	8	6.85	9.40	9.26
12/7/86	130318	F7	100	70.1	2316	6	7.76	9.57	9.16
12/7/86	141331	F6	68	73.4	2200	3	7.42	10.00	9.51
12/8/86	023909	F7	47	70.5	2323	6	7.29	9.37	8.96
12/10/86	015838	F7	69	68.0	2329	3	7.98	9.09	8.82
12/10/86	033900	F7	69	74.2	2312	4	7.35	9.23	8.19
12/11/86	064026	F7	147	73.3	2205	5	6.94	9.24	9.16
12/11/86	100150	F7	100	68.8	2218	10	6.51	9.08	9.01
12/11/86	193443	F6	213	73.4	2242	11	8.16	9.07	8.92
12/11/86	233157	F7	215	72.2	0125	2	7.49	9.66	9.51
12/12/86	043942	F7	314	73.7	2239	10	8.15	9.04	8.85
12/12/86	194746	F7	100	70.8	0100	2	7.18	9.45	9.30
12/13/86	110105	F7	69	71.2	2235	5	7.10	9.09	8.52
12/13/86	120654	F6	462	69.8	2042	11	8.16	9.39	9.30
12/13/86	124256	F7	147	67.5	2303	3	6.59	9.18	8.92
12/13/86	134734	F6	145	71.3	2116	15	7.48	9.53	9.13
12/13/86	134828	F6	46	69.3	2052	4	7.17	9.30	8.78
12/14/86	100211	F6	68	76.2	2030	1	8.19	9.45	9.22
12/14/86	215457	F6	145	75.1	2210	6	7.07	9.43	9.27
12/16/86	100048	F7	995	69.6	2215	11	8.12	9.38	9.36*

84

TABLE 11. Continued

Day	UT	Satellite	Φ (-volts)	MLAT	MLT	ΔT (sec)	Log₁₀ Ion Flux	Log₁₀ Electron Fluxes Total	≥9.6keV
12/16/86	110050	F6	213	75.0	2053	62	7.89	9.36	9.10
12/16/86	113924	F7	100	76.2	2249	3	6.58	9.23	8.89
12/16/86	174928	F6	100	67.9	2108	15	6.02	8.98	8.84
12/17/86	062014	F7	147	70.5	2204	4	7.04	8.89	8.80
12/17/86	172323	F6	213	74.8	0020	33	8.17	9.32	8.93
12/17/86	172443	F6	100	74.1	2309	15	6.41	9.39	8.71
12/20/86	134154	F7	147	69.2	2319	3	8.09	9.28	9.04
12/21/86	095802	F7	100	76.5	2207	3	7.99	9.98	9.30
12/21/86	225011	F6	68	72.8	2047	2	6.96	9.64	9.24
12/22/86	025740	F7	679	70.1	2300	11	7.90	9.70	9.58*
12/22/86	153937	F6	100	70.5	2119	8	7.59	9.39	9.30
12/23/86	001114	F6	145	72.5	1929	6	7.34	9.18	8.45
12/23/86	133501	F6	100	73.9	2152	2	7.82	9.66	9.64
12/23/86	142103	F7	69	71.7	2338	2	6.37	9.69	8.05
12/23/86	184029	F6	68	73.0	2226	21	6.75	8.63	8.45
12/24/86	031141	F6	213	70.5	1738	7	7.87	9.41	9.35
12/24/86	103934	F7	215	70.0	2223	2	7.03	9.24	8.93
12/24/86	121956	F7	100	71.0	2256	4	6.71	8.83	8.75
12/24/86	145700	F6	68	70.1	2103	2	6.26	8.93	8.75
12/24/86	214421	F6	68	73.4	2144	4	7.48	8.94	8.61
12/25/86	001225	F7	147	69.2	0027	3	6.67	9.09	8.98
12/25/86	051445	F7	215	83.4	2327	20	8.03	9.78	9.69
12/25/86	152228	F7	47	69.0	2342	2	6.82	8.86	8.81

TABLE 11. Continued

Day	UT	Satellite	Φ (-volts)	MLAT	MLT	ΔT (sec)	Log$_{10}$ Ion Flux	Log$_{10}$ Electron Fluxes Total	≥9.6keV
12/25/86	152249	F7	100	68.1	2337	8	7.22	9.05	7.75
12/25/86	161526	F6	100	73.2	2217	6	7.45	8.99	8.90
12/25/86	161549	F6	145	72.6	2204	22	7.78	9.17	9.09
12/26/86	022859	F6	100	72.4	1747	3	6.76	9.35	8.88
12/26/86	063911	F7	69	69.3	0002	1	6.84	9.61	9.47
12/26/86	072835	F6	100	74.5	1903	1	6.76	9.31	8.98
12/26/86	100004	F7	100	66.4	2211	18	7.61	9.24	8.24
12/26/86	155509	F6	100	71.1	2128	15	7.12	9.10	8.50
12/26/86	191741	F6	68	73.5	2237	1	7.60	9.87	9.25
12/26/86	205656	F6	317	76.5	0104	20	7.91	10.37	9.82
12/27/86	212711	F7	100	70.7	0106	3	6.52	9.64	9.59
12/28/86	041632	F7	47	74.8	2243	2	6.32	9.01	8.95
12/28/86	105732	F7	147	75.3	2226	4	6.97	9.30	7.88
12/28/86	165214	F6	68	73.8	2246	2	7.08	9.22	9.10
12/29/86	035610	F7	215	74.7	2252	15	7.72	9.11	8.88
12/31/86	122638	F6	68	71.1	2049	3	7.19	9.35	6.90
12/31/86	140702	F6	462	73.1	2141	21	8.08	9.67	9.63
12/31/86	140744	F6	145	71.7	2116	6	6.99	9.03	8.90
1/1/87	025314	F7	69	76.9	0004	1	7.00	9.20	9.11
1/1/87	111949	F7	69	65.3	2230	1	6.37	9.04	8.38
1/1/87	153008	F6	68	66.2	2025	14	6.30	9.05	8.85*
1/1/87	212809	F7	314	66.4	0014	4	8.25	9.52	9.20
1/1/87	221611	F6	68	74.3	2130	15	6.69	8.72	8.66

TABLE 11. Continued

Day	UT	Satellite	Φ (-volts)	MLAT	MLT	ΔT (sec)	Log_{10} Ion Flux	Log_{10} Electron Fluxes Total	≥9.6keV
1/1/87	221643	F6	145	73.2	2113	22	7.52	8.86	8.82
1/2/87	091756	F7	215	69.5	2157	5	6.95	9.11	8.83
1/2/87	201148	F6	68	72.7	2204	17	6.87	8.81	8.64
1/3/87	085735	F7	462	70.1	2152	8	7.79	9.23	9.04
1/3/87	103717	F7	69	72.2	2215	2	6.86	8.82	8.42
1/3/87	121809	F7	147	71.6	2252	3	7.79	9.19	8.96
1/3/87	144407	F6	46	73.1	2152	2	6.21	9.76	7.60
1/3/87	144505	F6	46	71.4	2118	2	6.52	8.72	8.30
1/4/87	000905	F7	147	72.8	0110	4	6.98	9.54	9.32
1/4/87	000957	F7	314	71.0	0043	25	7.98	9.30	9.24*
1/5/87	182226	F7	147	71.0	0035	3	6.76	9.53	9.31
1/6/87	111656	F7	69	72.6	2228	6	7.43	9.08	8.00
1/6/87	162108	F7	47	69.5	2355	1	7.91	9.68	7.43
1/7/87	160029	F7	69	70.0	2353	2	6.77	9.40	8.97
1/9/87	083704	F7	462	68.3	2147	6	7.72	9.35	9.29
1/9/87	091337	F6	145	74.6	1943	15	7.61	9.57	9.53
1/9/87	101521	F7	215	75.2	2203	3	7.23	9.14	8.81
1/9/87	115654	F7	147	71.9	2241	8	7.78	9.29	9.08
1/9/87	123540	F6	314	73.6	2117	30	7.64	9.44	9.29
1/9/87	133832	F7	47	69.4	2309	1	5.71	8.59	8.08
1/9/87	152011	F7	69	68.4	2330	2	7.46	9.03	8.63
1/9/87	234813	F7	47	71.1	0051	2	6.42	8.95	8.31
1/10/87	081506	F7	47	74.6	2140	4	6.84	8.62	8.40

TABLE 11. Continued

Day	UT	Satellite	Φ (-volts)	MLAT	MLT	ΔT (sec)	Log_{10} Ion Flux	Log_{10} Electron Fluxes	
								Total	≥9.6keV
1/10/87	081542	F7	147	72.4	2142	15	7.10	8.37	7.84
1/10/87	081559	F7	314	71.5	2142	7	8.03	9.24	8.98
1/11/87	043525	F7	314	71.9	2213	52	7.87	8.74	8.12
1/11/87	180100	F7	314	71.2	0032	3	7.68	9.61	9.58
1/11/87	180117	F7	147	70.6	0023	11	7.50	8.78	8.71
1/12/87	004741	F7	679	75.2	0135	4	7.39	9.78	9.66
1/12/87	163636	F6	100	71.9	2142	15	5.85	8.67	8.44
1/13/87	053446	F7	47	73.8	2201	3	7.09	9.85	7.40
1/13/87	121734	F7	69	67.9	2242	1	6.05	8.97	8.77
1/13/87	143339	F6	145	71.9	2117	4	7.25	8.91	7.53
1/14/87	065551	F7	69	69.7	2143	1	7.29	8.97	7.46
1/17/87	004929	F7	462	69.9	0008	22	8.12	9.22	9.11
1/17/87	041130	F7	47	79.4	2317	2	6.24	8.96	8.73
1/17/87	071516	F7	47	69.2	2140	1	6.44	9.18	8.72
1/18/87	222549	F7	47	68.1	0027	1	7.12	8.72	8.42
1/19/87	083432	F7	462	71.2	2139	4	7.15	8.91	8.79
1/19/87	104410	F6	46	71.9	2009	4	6.77	9.15	7.55
1/19/87	154829	F6	46	71.0	2116	4	6.59	9.01	8.20
1/19/87	154843	F6	46	70.5	2108	2	6.04	9.02	8.32
1/20/87	152719	F6	100	70.5	2103	28	7.54	9.66	9.23
1/21/87	132326	F6	145	72.6	2111	3	7.51	9.69	9.38
1/21/87	182939	F6	46	69.7	2115	1	6.66	9.74	8.88
1/22/87	180654	F6	46	72.2	2157	2	6.44	9.28	8.96

TABLE 11. Continued

Day	UT	Satellite	Φ (-volts)	MLAT	MLT	ΔT (sec)	Log_{10} Ion Flux	Log_{10} Electron Fluxes Total	$\geq 9.6 keV$
1/23/87	035245	F7	69	72.0	2227	13	6.55	8.85	8.54
1/23/87	053335	F7	100	72.2	2154	5	7.51	8.92	8.85
1/23/87	085241	F7	47	75.7	2135	2	6.43	9.09	8.73
1/23/87	103317	F7	215	74.6	2202	14	8.12	9.08	9.04*
1/23/87	110005	F6	46	71.3	2011	2	6.23	9.38	9.14
1/23/87	121545	F7	69	68.3	2237	2	6.65	8.74	8.67
1/23/87	124148	F6	213	70.0	2032	21	7.30	9.42	9.19
1/23/87	160444	F6	145	70.0	2103	3	6.27	9.48	9.19
1/23/87	225300	F6	68	74.3	2050	6	7.14	8.91	8.70
1/24/87	065355	F7	147	70.6	2138	3	7.00	9.65	9.04*
1/24/87	085638	F6	46	75.3	1927	1	6.56	8.73	8.35
1/24/87	133412	F7	215	74.8	2322	9	7.66	8.88	8.82
1/24/87	172409	F6	46	71.7	2142	8	7.03	8.50	8.40
1/24/87	172436	F6	46	70.8	2125	1	5.78	8.39	8.14
1/24/87	172513	F6	462	69.4	2106	23	7.92	9.11	8.85
1/25/87	045132	F7	47	77.0	2224	2	7.25	9.01	8.94
1/25/87	081356	F7	100	69.6	2135	11	6.71	8.65	7.22
1/26/87	111407	F7	47	70.5	2216	2	6.15	8.87	8.61
1/26/87	131920	F6	46	69.2	2030	3	6.69	9.59	9.15
1/27/87	041238	F7	1430	71.3	2214	11	8.02	8.75	8.68*
1/28/87	035138	F7	69	72.7	2230	2	6.28	8.78	8.63
1/28/87	103239	F7	147	73.6	2200	10	7.68	9.11	9.03
1/28/87	174052	F6	100	69.8	2112	10	6.87	8.84	8.58

TABLE 11. Continued

Day	UT	Satellite	Φ (-volts)	MLAT	MLT	ΔT (sec)	Log_{10} Ion Flux	Log_{10} Electron Fluxes	
								Total	$\geq 9.6keV$
1/29/87	115411	F7	462	69.4	2229	3	7.88	9.81	9.70
1/29/87	121320	F6	213	73.4	2054	13	7.08	9.60	9.23
1/29/87	133427	F7	147	71.4	2307	7	7.05	9.16	9.10
1/29/87	151611	F7	314	69.8	2333	10	8.01	8.81	8.71
1/30/87	012648	F7	100	73.8	0031	4	6.67	9.27	9.25
1/30/87	131422	F7	462	70.4	2257	4	8.13	10.03	9.43
1/31/87	025005	F7	314	71.9	2304	8	6.97	9.07	8.96
1/31/87	075144	F7	215	73.7	2130	3	7.89	9.25	9.17
1/31/87	093207	F7	100	72.7	2141	6	7.34	9.37	6.86

Appendix B: Charging Time History

for Select Events

The summary of charging events in Appendix A lists parameters only for the time of an event's peak potential. To illustrate a more complete picture, Figures 21-24 depict the satellite potentials and electron fluxes during five charging events from their beginning to end. The cases are unique and illustrate the results described in Chapter VI.

The duration of the charging event shown in Figure 21 is one of the longest identified in this study. Potential levels exceed -300 volts three times. During the first 20 seconds of the event, rapid changes in the charging levels closely correspond to rapid changes in the ≥ 9.6 keV electron fluxes. This feature is less evident during much of the remaining event. Charging is poorly correlated to total electron flux; total electron fluxes are greatest toward the end of the event when potentials decrease to zero.

Figure 22 differs from Figure 21 in that both the total and energetic electron fluxes are 10 to 100 times greater than those in Figure 21, but similar charging levels occur. Such an increase in lower energy electron fluxes could significantly increase secondary electron production and inhibit charging. The peak potential of -462 volts forms when the total electron flux consists almost entirely of electrons ≥ 9.6 keV.

The two most severe charging events identified in this study are shown in Figure 23. In both cases, significant electron fluxes extend beyond the energy range (30 keV) of the detector. Charging levels reach -1.0 kilovolt on two occasions in the bottom plot and -1.4 kilovolts in the top plot and occur when the total flux consists entirely of energetic electrons. However, charging is less severe at other times during both events when these energetic electron fluxes are equal or greater. An increased ambient plasma density could be responsible for the lower potential levels during these periods.
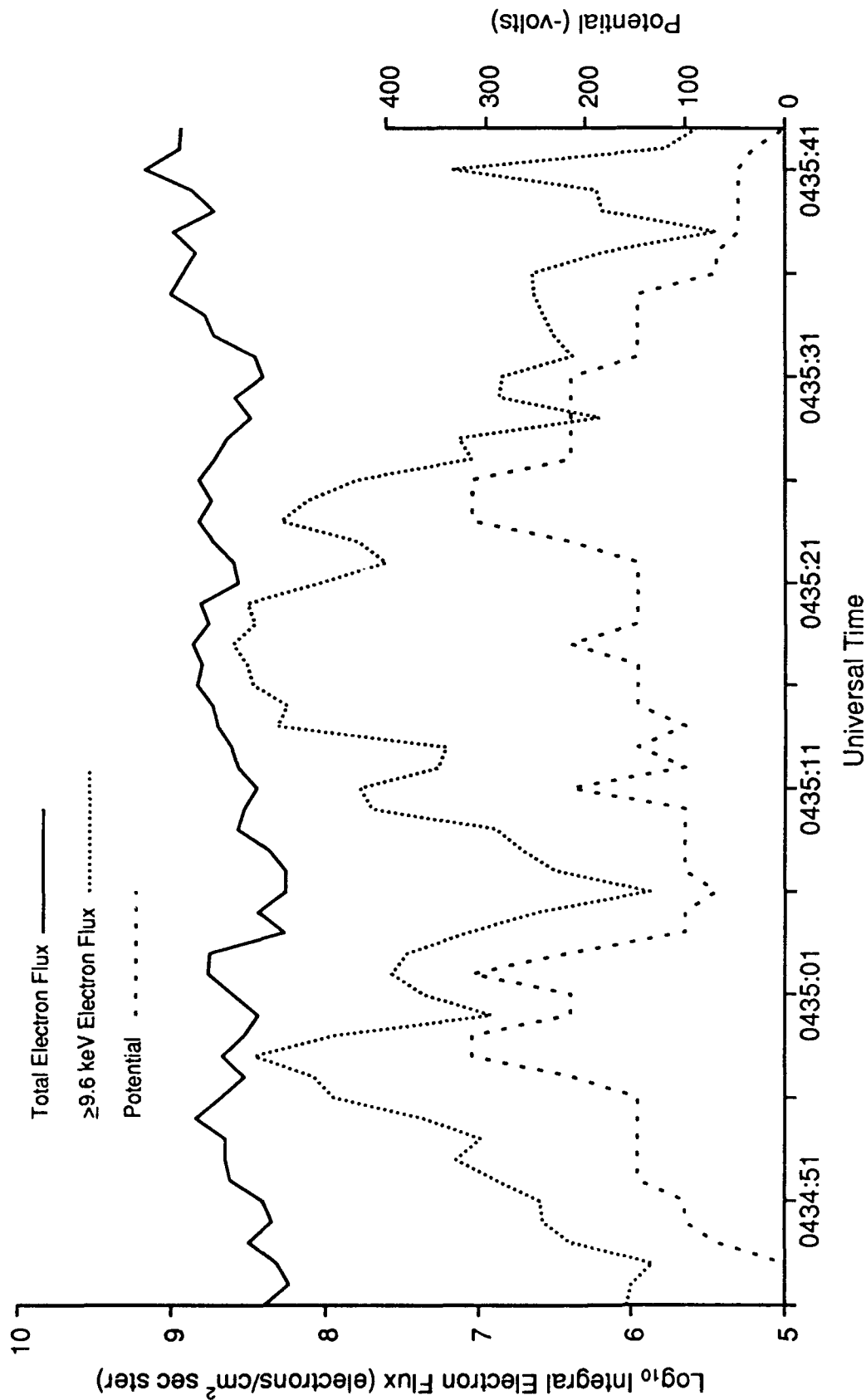
Fig. 21. The electron integral number flux for the SSJ/4 total energy range (solid line) and for energies ≥9.6 keV (dotted line), and the DMSP F7 satellite potential (dashed line) during a charging event on January 11, 1987.
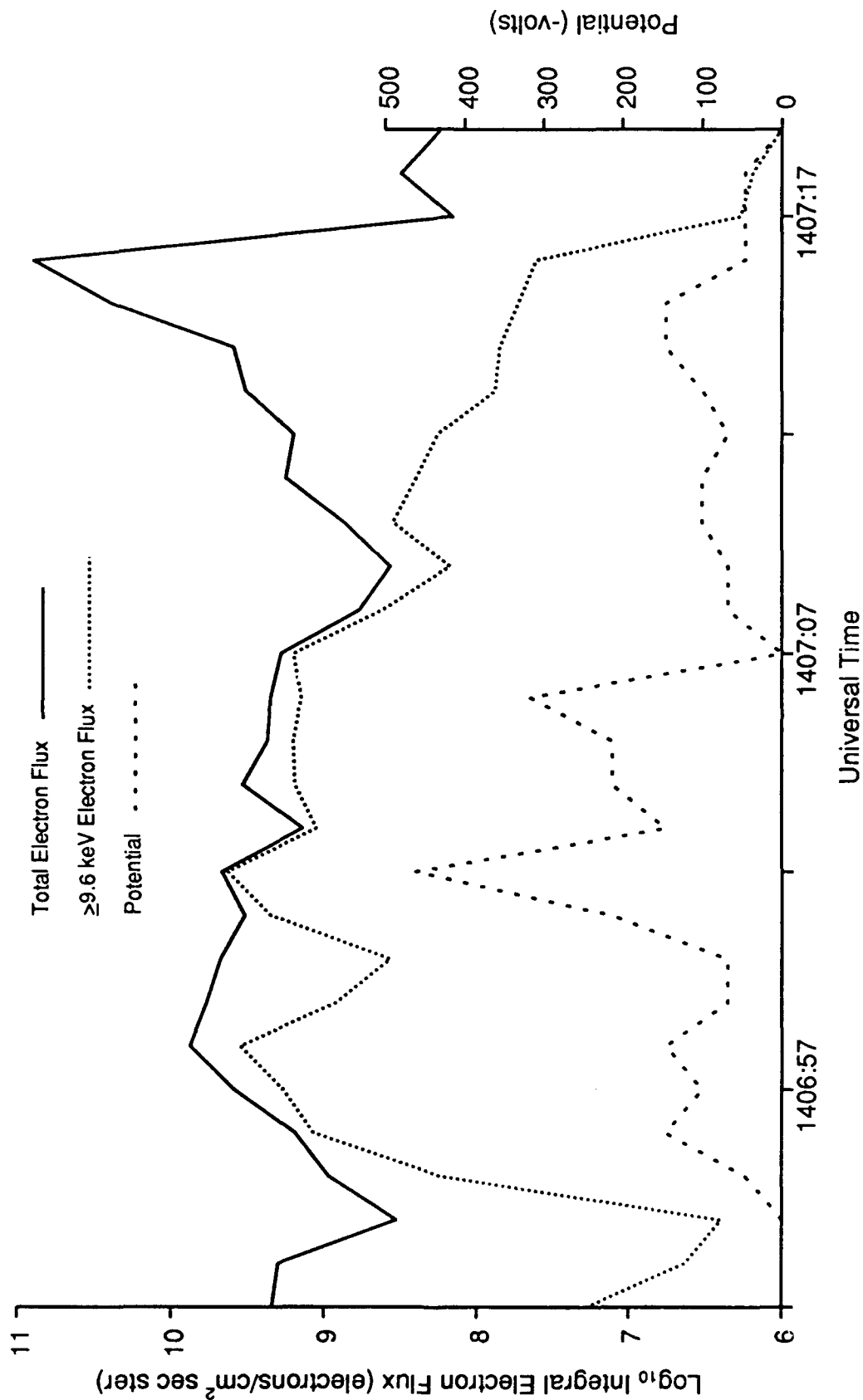
Fig. 22. The electron integral number flux for the SSJ/4 total energy range (solid line) and for energies ≥9.6 keV (dotted line), and the DMSP F6 satellite potential (dashed line) during a charging event on December 31, 1986.
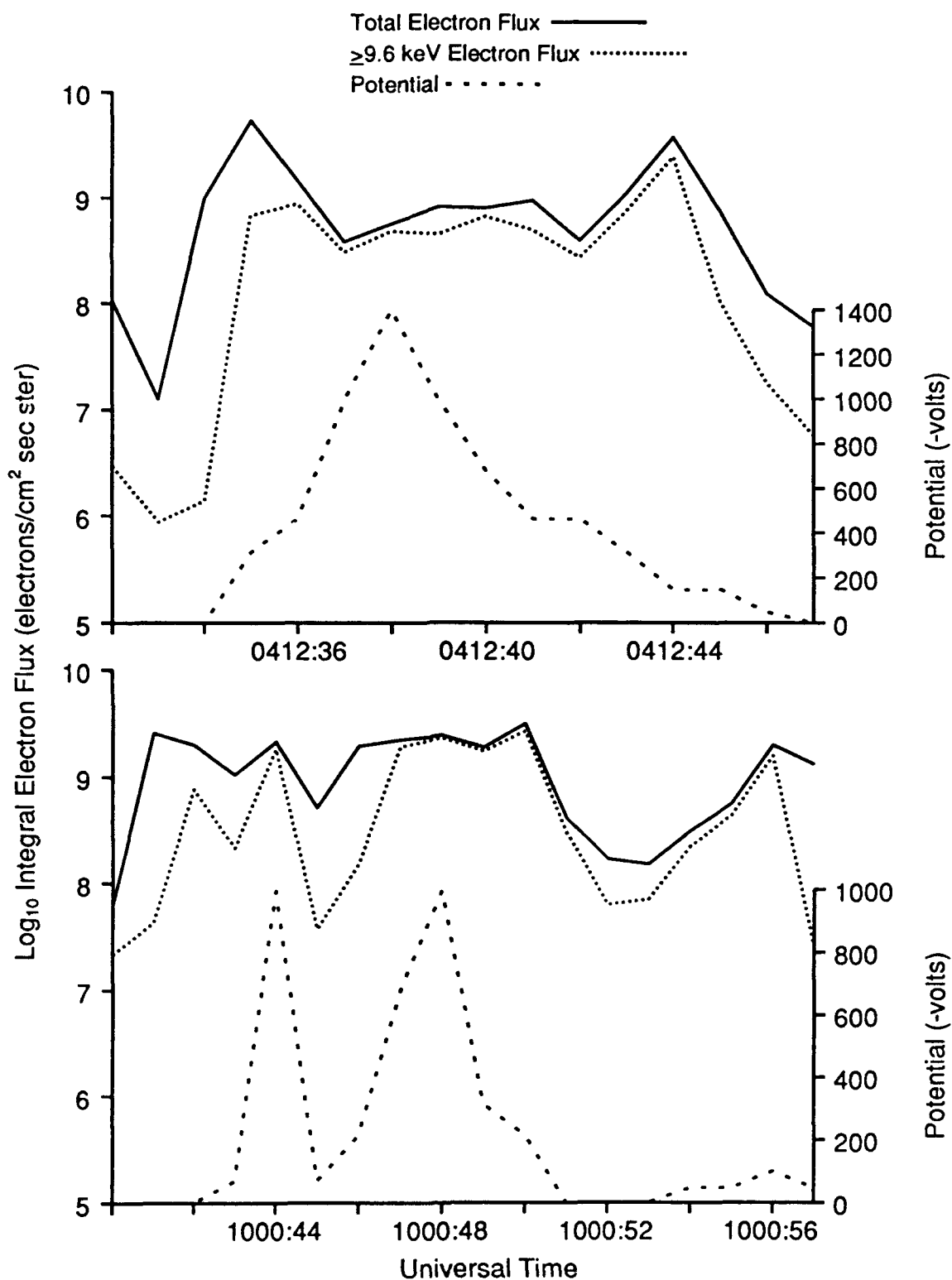
Fig. 23. The electron integral number flux for the SSJ/4 total energy range (solid line) and for energies ≥9.6 keV (dotted line), and the DMSP F7 satellite potential (dashed line) during severe charging events on January 27, 1987, (top) and December 16, 1986, (bottom).
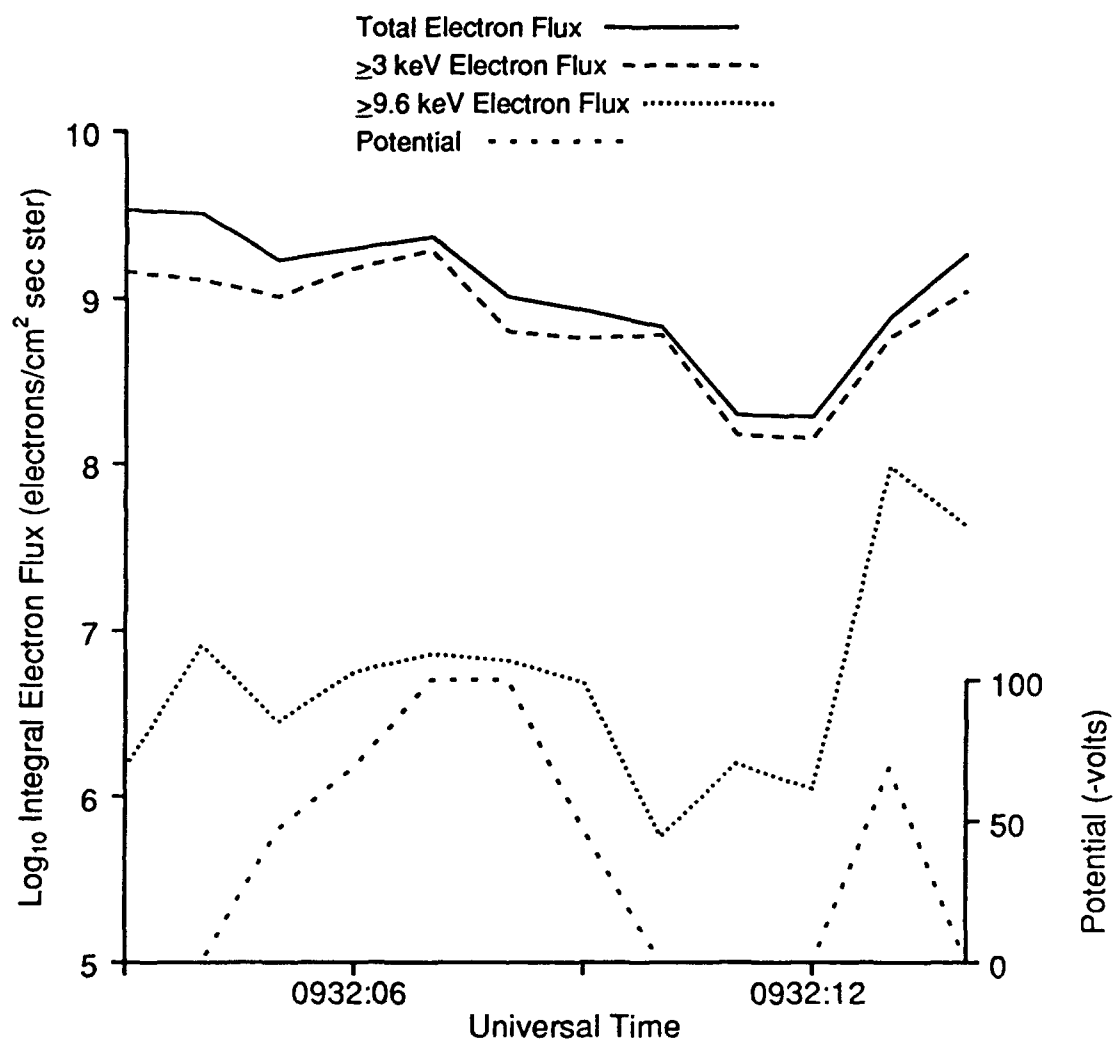
Fig. 24. The electron integral number flux for the SSJ/4 total energy range (solid line), for energies ≥3 keV (long dashes), and for energies ≥9.6 keV (dotted line), and the DMSP F7 satellite potential (short dashes) during a charging event on January 31, 1987.

Finally, Figure 24 illustrates a less severe charging case when ≥9.6 keV electron fluxes are relatively low. The electron fluxes above 3 keV are significantly greater and contribute to nearly all of the total electron flux when the satellite fir; t charges to -100 volts. While the ≥9.6 keV electrons contribute to a charge imbalance, their fluxes are too low to generate charging at this level. Moreover, charging was not identified when ≥9.6 keV electron fluxes were this low unless significant fluxes of lower energy electrons (2-6 keV) were present.

Appendix C: SSJ/4 Count Rate Conversion Factors

The energy channel configurations and count rate conversion factors for the DMSP F6, F7, F8, and F9 SSJ/4 instruments are shown in Tables 12, 13, 14, and 15 respectively. The factors ($\log_{10}$) shown may be multiplied by the measured particle count in each channel to obtain a differential number flux (C-FLX) in particles/(cm^2 sec ster keV), an integral number flux (C-NFLX) in particles/(cm^2 sec ster), and a distribution function (D-DIST) in sec^3/cm^6. The factors are a result of particle beam and in-flight calibrations and were provided by the Space Particles Environment Branch of the Geophysics Laboratory Space Physics Division.

TABLE 12. DMSP F6 SSJ/4 Energy Channel Configuration and Factors (Log_{10}) which Convert Count Rates to Various Quantities

Channel	Central Energy(eV)	Electron Sensor			Ion Sensor	
		C-FLX	C-NFLX	C-DIST	C-NFLX	C-DIST
1	30,180	4.134	5.114	-34.140	4.734	-27.996
2	20,620	4.318	5.225	-33.790	4.836	-27.652
3	14,040	4.396	5.137	-33.547	4.842	-27.315
4	9,580	4.490	5.068	-33.287	4.844	-26.979
5	6,500	4.577	4.989	-33.031	4.841	-26.652
6	4,420	4.687	4.923	-32.754	4.831	-26.320
7	3,050	4.805	4.877	-32.475	4.825	-26.000
8	2,060	4.895	4.809	-32.214	4.843	-25.652
9	1,410	5.025	4.757	-31.917	4.831	-25.317
10	984	5.127	4.691	-31.660	4.823	-25.000
11	992	5.863	5.425	-30.928	3.210	-26.618
12	679	6.009	5.431	-30.618	3.255	-26.267
13	462	6.107	5.364	-30.354	3.121	-26.070
14	317	6.301	5.396	-29.996	3.207	-25.658
15	213	6.477	5.412	-29.646	3.204	-25.328
16	145	6.708	5.459	-29.249	3.193	-24.987
17	100	7.009	5.594	-28.785	3.196	-24.658
18	68	7.310	5.741	-28.318	3.185	-24.347
19	46	7.708	5.963	-27.750	3.185	-24.001
20	32	8.210	6.356	-27.091	3.253	-23.668

TABLE 13. DMSP F7 SSJ/4 Energy Channel Configuration and Factors (Log_{10}) which Convert Count Rates to Various Quantities

Channel	Central Energy(eV)	Electron Sensor			Ion Sensor	
		C-FLX	C-NFLX	C-DIST	C-NFLX	C-DIST
1	30,340	4.246	5.228	-34.032	4.612	-28.121
2	20,710	4.318	5.228	-33.793	4.715	-27.780
3	14,070	4.396	5.143	-33.547	4.713	-27.449
4	9,570	4.490	5.064	-33.286	4.708	-27.115
5	6,570	4.577	4.984	-33.035	4.699	-26.793
6	4,470	4.687	4.932	-32.759	4.710	-26.453
7	3,050	4.805	4.879	-32.475	4.702	-26.123
8	2,100	4.895	4.803	-32.223	4.687	-25.812
9	1,430	5.025	4.773	-31.924	4.713	-25.456
10	985	5.127	4.702	-31.660	4.702	-25.133
11	995	5.490	5.064	-31.303	3.260	-26.578
12	679	5.611	5.037	-31.016	3.288	-26.237
13	462	5.708	4.969	-30.752	3.279	-25.914
14	314	5.895	4.986	-30.397	3.281	-25.575
15	215	6.049	4.971	-30.078	3.267	-25.254
16	147	6.246	5.004	-29.717	3.276	-24.917
17	100	6.477	5.068	-29.318	3.279	-24.582
18	69	6.708	5.130	-28.924	3.255	-24.274
19	47	6.968	5.236	-28.500	3.276	-23.932
20	32	7.253	5.430	-28.047	3.340	-23.609

TABLE 14. DMSP F8 SSJ/4 Energy Channel Configuration and Factors (Log$_{10}$) which Convert Count Rates to Various Quantities

Channel	Central Energy(eV)	Electron Sensor			Ion Sensor	
		C-FLX	C-NFLX	C-DIST	C-NFLX	C-DIST
1	31,300	4.496	5.504	-33.796	4.957	-27.815
2	21,100	4.569	5.498	-33.550	5.053	-27.469
3	14,300	4.647	5.401	-33.304	5.041	-27.138
4	9,720	4.742	5.326	-33.041	5.037	-26.804
5	6,610	4.827	5.243	-32.788	5.029	-26.478
6	4,500	4.937	5.188	-32.511	5.033	-26.137
7	3,050	5.057	5.140	-32.224	5.033	-25.804
8	2,070	5.146	5.061	-31.967	5.013	-25.487
9	1,400	5.276	5.025	-31.664	5.033	-25.128
10	950	5.378	4.958	-31.395	5.025	-24.799
11	950	5.504	5.083	-31.269	3.543	-26.282
12	640	5.623	5.029	-30.979	3.545	-25.936
13	440	5.721	4.939	-30.717	3.511	-25.618
14	310	5.908	4.969	-30.378	3.526	-25.293
15	210	6.061	4.981	-30.056	3.543	-24.967
16	144	6.258	5.004	-29.695	3.542	-24.633
17	98	6.490	5.072	-29.296	3.543	-24.296
18	68	6.721	5.143	-28.907	3.533	-23.991
19	45	6.980	5.246	-28.469	3.553	-23.636
20	31	7.267	5.412	-28.020	3.587	-23.319

TABLE 15. DMSP F9 SSJ/4 Energy Channel Configuration and Factors (Log_{10}) which Convert Count Rates to Various Quantities

Channel	Central Energy(eV)	Electron Sensor C-FLX	Electron Sensor C-NFLX	Electron Sensor C-DIST	Ion Sensor C-NFLX	Ion Sensor C-DIST
1	31,300	4.706	5.714	-33.585	4.960	-27.812
2	21,100	4.778	5.708	-33.341	5.057	-27.465
3	14,300	4.857	5.612	-33.093	5.045	-27.134
4	9,720	4.948	5.533	-32.836	5.041	-26.799
5	6,610	5.037	5.453	-32.578	5.029	-26.474
6	4,500	5.146	5.396	-32.302	5.037	-26.135
7	3,050	5.265	5.348	-32.015	5.037	-25.801
8	2,070	5.354	5.272	-31.757	5.017	-25.483
9	1,400	5.486	5.236	-31.455	5.037	-25.124
10	950	5.588	5.167	-31.186	5.029	-24.796
11	950	5.415	4.994	-31.359	3.474	-26.351
12	640	5.534	4.941	-31.067	3.479	-26.002
13	440	5.632	4.849	-30.807	3.444	-25.684
14	310	5.818	4.879	-30.469	3.459	-25.360
15	210	5.975	4.894	-30.142	3.474	-25.034
16	144	6.170	4.918	-29.783	3.476	-24.699
17	98	6.401	4.981	-29.385	3.474	-24.365
18	68	6.632	5.057	-28.996	3.465	-24.058
19	45	6.892	5.158	-28.558	3.486	-23.703
20	31	7.179	5.324	-28.109	3.520	-23.386